nature aging

Letter

https://doi.org/10.1038/s43587-024-00641-z

Identification of a longevity gene through evolutionary rate covariation of insect mito-nuclear genomes

Received: 3 July 2023

Accepted: 2 May 2024

Published online: 04 June 2024

Check for updates

Mei Tao[1,2,3,9], Jiani Chen[1,9], Chunlai Cui[4,9], Yandong Xu[5,6,9], Jingxiu Xu[5], Zheyi Shi[1], Jiaqi Yun[4], Junwei Zhang[1], Guo-Zheng Ou[1], Chao Liu[1], Yun Chen[1], Zeng-Rong Zhu[1], Ronghui Pan[7], Suhong Xu[5], Xue-xin Chen[1], Antonis Rokas[8], Yang Zhao[5,6], Sibao Wang[4] ✉, Jianhua Huang[1] ✉ & Xing-Xing Shen[1,2,3] ✉

Oxidative phosphorylation, essential for energy metabolism and linked to the regulation of longevity, involves mitochondrial and nuclear genes. The functions of these genes and their evolutionary rate covariation (ERC) have been extensively studied, but little is known about whether other nuclear genes not targeted to mitochondria evolutionarily and functionally interact with mitochondrial genes. Here we systematically examined the ERC of mitochondrial and nuclear benchmarking universal single-copy ortholog (BUSCO) genes from 472 insects, identifying 75 non-mitochondria-targeted nuclear genes. We found that the uncharacterized gene *CG11837*—a putative ortholog of human *DIMT1*—regulates insect lifespan, as its knockdown reduces median lifespan in five diverse insect species and *Caenorhabditis elegans*, whereas its overexpression extends median lifespans in fruit flies and *C. elegans* and enhances oxidative phosphorylation gene activity. Additionally, *DIMT1* overexpression protects human cells from cellular senescence. Together, these data provide insights into the ERC of mito-nuclear genes and suggest that *CG11837* may regulate longevity across animals.

Animal cells contain both nuclear and mitochondrial genomes in spatially distinct compartments. In a single cell, mitochondrial genomes are typically present at hundreds to thousands of copies, whereas the nuclear genome typically has two copies. The mitochondrial genome often encodes 37 genes and accounts for approximately 0.25% of the entire cell's genetic makeup[1], whereas the nuclear genome often encodes tens of thousands of genes and accounts for approximately 99.75% of the cell's genetic makeup[1]. Coordination between mitochondrial and nuclear genomes is crucial for cellular functions[2], notably in the oxidative phosphorylation (OXPHOS) pathway, which generates ATP and contains five protein complexes encoded by all 13 mitochondrial protein-coding genes (mtOXPHOS) and approximately 70 nuclear protein-coding genes (nuOXPHOS). Dysfunctions of these mtOXPHOS and nuOXPHOS genes in model species lead to multisystem diseases[3], including, but not limited to, aging-related diseases[4], neurodegenerative disorders[5] and metabolic disorders[6].

[1]Key Laboratory of Biology of Crop Pathogens and Insects of Zhejiang Province, College of Agriculture and Biotechnology, Zhejiang University, Hangzhou, China. [2]Hainan Institute, Zhejiang University, Yazhou Bay Science and Technology City, Sanya, China. [3]Centre for Evolutionary and Organismal Biology, Zhejiang University, Hangzhou, China. [4]New Cornerstone Science Laboratory, CAS Key Laboratory of Insect Developmental and Evolutionary Biology, CAS Center for Excellence in Molecular Plant Sciences, Shanghai Institute of Plant Physiology and Ecology, Chinese Academy of Sciences, Shanghai, China. [5]Zhejiang University School of Medicine, Hangzhou, China. [6]Zhejiang Provincial Key Lab of Genetic and Developmental Disorders, Hangzhou, China. [7]ZJU-Hangzhou Global Scientific and Technological Innovation Center, Zhejiang University, Hangzhou, China. [8]Department of Biological Sciences and Evolutionary Studies Initiative, Vanderbilt University, Nashville, TN, USA. [9]These authors contributed equally: Mei Tao, Jiani Chen, Chunlai Cui, Yandong Xu. ✉e-mail: sbwang@cemps.ac.cn; jhhuang@zju.edu.cn; xingxingshen@zju.edu.cn

Recent studies employed genome-scale data to investigate the evolutionary rate covariation (ERC) of nuOXPHOS genes and mtOXPHOS genes in different lineages, including mammals[7], bivalves[8] and insects[9]. Despite using moderate numbers of genomes (mammals: 58 species; bivalves: 31 species; insects: 44 species), these studies found highly correlated evolutionary rates between nuOXPHOS genes and mtOXPHOS genes. nuOXPHOS genes also showed stronger signals of covariation with mtOXPHOS genes compared to other nuclear-encoded mitochondrial (nuMT) genes[2,10]. In addition to the mitochondria-targeted nuclear (nuOXPHOS and nuMT) genes, other nuclear genes (for example, *SIRT1* in human) that are not targeted to mitochondria were previously reported to severely affect mitochondrial functions and phenotypes[11]. What remains unknown is how many other nuclear genes are not targeted to mitochondria but exhibit strong signals of ERC with mtOXPHOS genes and functionally associate with them.

To address this gap, we systematically examined the ERC of 1,203 conserved non-mitochondria-targeted nuclear genes and 67 nuOXPHOS genes with 13 mtOXPHOS genes using the high-quality nuclear and mitochondrial genomes of 472 insects, representing 19 of 23 species-rich orders[12]. We asked three questions. (1) What is the landscape of ERC signals of all non-mitochondria-targeted nuclear genes and all nuOXPHOS genes with the 13 mtOXPHOS genes? (2) Which are the non-mitochondria-targeted nuclear genes that exhibit strong ERC with the mtOXPHOS genes? (3) What are the biological functions of non-mitochondria-targeted nuclear genes that exhibit strong ERC with the mtOXPHOS genes? Our study identified 75 non-mitochondria-targeted nuclear genes exhibiting strong ERC signals with mtOXPHOS genes and displaying diverse functions, such as ribosome biogenesis, DNA replication and telomere maintenance. Additionally, we discovered *CG11837*, a longevity gene putatively considered an ortholog of the human gene *DIMT1*, contributing to lifespans from worms to insects and protecting human cells from cellular senescence.

Results

Evolution of nuclear and mitochondrial genomes in insects

To examine the modes of nuclear and mitochondrial genome evolution in insects, we compiled 472 mitochondrial and nuclear genomes (Methods and Supplementary Table 1). These 472 insects represent 19 of 23 species-rich orders[12]. Analysis of nuclear genome assembly completeness revealed that 357 of 472 (~76%) nuclear genomes have at least 90% of the 1,417 full-length benchmarking universal single-copy ortholog (BUSCO) nuclear genes (Supplementary Fig. 1). The percentage of complete BUSCO genes varied between 22.2% and 99.9%, with an average value of 89.3%. Regarding mitochondrial genomes, 440 genomes (~93%) contained all 13 protein-coding genes (PCGs), whereas nearly all genomes had at least 10. Examining gene composition (Supplementary Fig. 2), four genes (*COX3*, *CYTB*, *ND4* and *ND5*) were universally present, whereas eight (*ATP6*, *COX1*, *COX2*, *ND1*, *ND2*, *ND3*, *ND4L* and *ND6*) were sporadically absent in 1–6 unrelated species. *ATP8* was the most commonly absent gene, being absent in 25 out of 472 species. The absence of the *ATP8* gene is likely attributed to its small size and high variation in base composition that could pose challenges for its annotations.

We next inferred two concatenation-based maximum likelihood (ML) phylogenies of 472 insects and 15 outgroups using the 1,417 nuclear BUSCO (nuBUSCO) PCGs and 13 mitochondrial protein-coding genes (mtPCGs), respectively. Most internodes in both nuBUSCO (98%) and mtPCG (84%) phylogenies received strong (≥95%) support (Supplementary Figs. 3 and 4). However, the nuBUSCO phylogeny was more congruent with a previous genome-scale phylogeny of 126 insects[13] than the mtPCG phylogeny (Extended Data Fig. 1). The nuBUSCO phylogeny supported the monophyly of 19 orders, with intraordinal relationships consistent with a previous study[13], except for the placement of the order Phthiraptera (Fig. 1a). In our nuBUSCO phylogeny, Phthiraptera was recovered as the sister group to Thysanoptera, albeit with low branch support (bootstrap value = 56%). In contrast, a previous genome-scale study supported (bootstrap value = 89%) the Phthiraptera as the sister group to the holometabolous insects[13]. The conflicting placement of the Phthiraptera likely results from our nuBUSCO phylogeny containing only one taxon (*Pediculus humanus*) in Phthiraptera, whereas the previous genome-scale study included four taxa. In addition, the mtPCG phylogeny did not support the monophyly of each of three orders (Ephemeroptera, Hemiptera and Coleoptera), likely due to fewer markers and sites, maternal inheritance, stronger base composition bias and/or higher substitution rate heterogeneity.

To quantify the similarities and differences in the modes of nuclear and mitochondrial insect genome evolution, we assessed GC content and evolutionary rate across 472 insects. Surprisingly, nuclear genomes generally exhibited higher GC content than their mitochondrial genomes (Fig. 1a), with ratios ranging from 0.8 to 3.3 and an average of 1.7. Additionally, the five largest orders— Hemiptera, Hymenoptera, Coleoptera, Lepidoptera and Diptera—displayed significant differences in GC content between nuclear and mitochondrial genomes (Supplementary Fig. 5a). When examining the GC content correlation between nuclear and mitochondrial genomes for each of the five largest orders, positive correlations were observed in some orders but not in others (Supplementary Fig. 5b). To calculate the evolutionary rate for each species, we used a sum of path distances from the most recent common ancestor of insects to its tip in the ML tree. Because the nuBUSCO phylogeny was more congruent with a previous genome-scale study[13] than the mtPCG phylogeny, we used the topology constrained to recover the nuBUSCO phylogeny (Fig. 1a) to re-estimate all branch lengths for the mtPCG data matrix (Fig. 1a). The comparisons of evolutionary rate of nuclear and mitochondrial genomes showed order-specific differences among the five largest orders (Fig. 1c). These order-specific differences in evolutionary rate

Fig. 1 | Contrasting patterns of genomic properties between nuclear and mitochondrial genomes in insects. We sampled the high-quality nuclear and mitochondrial genomes of 472 insects (Supplementary Table 1), representing 19 of 23 species-rich orders (that is, orders with >500 described species)[12]. **a**, The upper phylogeny was a concatenated ML tree inferred from analysis of 1,417 nuBUSCO PCGs under a single LG + G4. The complete phylogenetic relationships of 472 insects in the nuBUSCO phylogeny are given in Supplementary Fig. 3. Because the topology of the ML phylogeny inferred from all 13 mtPCGs was largely incongruent with that of the nuBUSCO phylogeny, we present the lower phylogeny constrained to recover the nuBUSCO phylogeny, but we re-estimated all their branch lengths using the mtPCG data matrix under a single mtInv+F + G4. The complete phylogenetic relationships of 472 insects in the unconstrained mtPCG phylogeny are shown in Supplementary Fig. 4. The concentric track on the periphery of the figure depicts GC content (%) of nuclear and mitochondrial genomes, respectively. Images representing taxa were taken from the free-to-use PhyloPic website (http://phylopic.org)[58]. **b**, Comparison of GC content between mitochondrial (*x* axis) and nuclear (*y* axis) genomes across 472 insects. Each dot corresponds to one species ($n = 472$). **c**, Comparison of evolutionary rate between mitochondrial (*x* axis) and nuclear (*y* axis) genomes across 472 insects. Each dot corresponds to one species ($n = 472$). For a given species, the evolutionary rates of its nuclear genome and mitochondrial genome were the sums of path distances from the most recent common ancestor of insects to its tip in the nuBUSCO phylogeny (upper phylogeny in **a**) and in the constrained mtPCG phylogeny (lower phylogeny in **a**), respectively. Because the five largest orders (Lepidoptera, Coleoptera, Diptera, Hemiptera and Hymenoptera) constitute 428 (~91%) of the 472 insects, we also assessed differences in GC content and evolutionary rate and explored their correlations between nuclear and mitochondrial genomes within each of these five largest orders (Supplementary Figs. 5 and 7).

https://doi.org/10.1038/s43587-024-00641-z

still held (Supplementary Fig. 6) with unconstrained mtPCG phylogeny (Supplementary Fig. 4). Specifically, Hemiptera and Hymenoptera nuclear genomes evolved slower than their mitochondrial genomes, whereas the opposite trend was observed in Coleoptera, Lepidoptera and Diptera (Supplementary Fig. 7a). When investigating the evolutionary rate correlation between nuclear and mitochondrial genomes, we

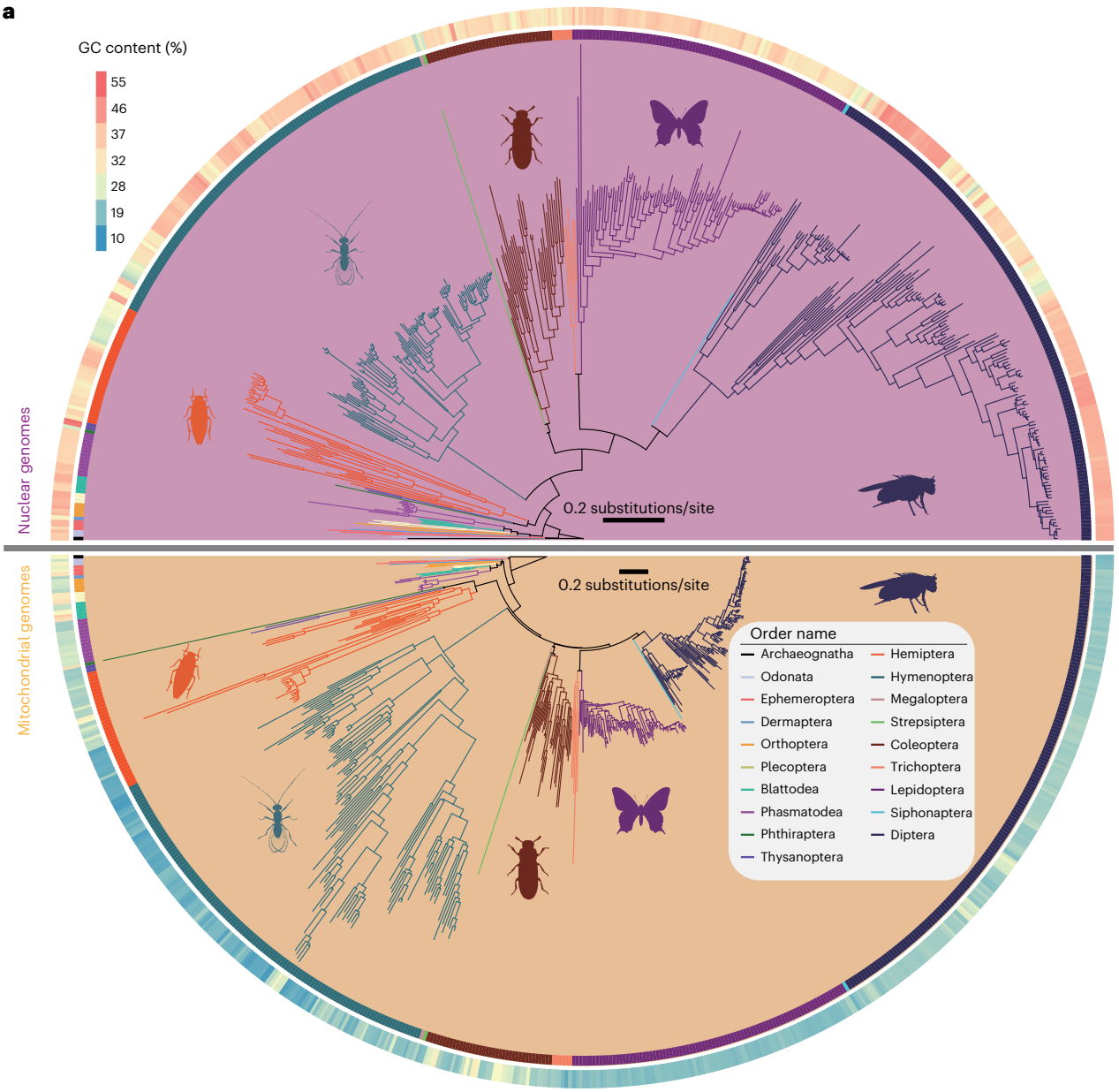

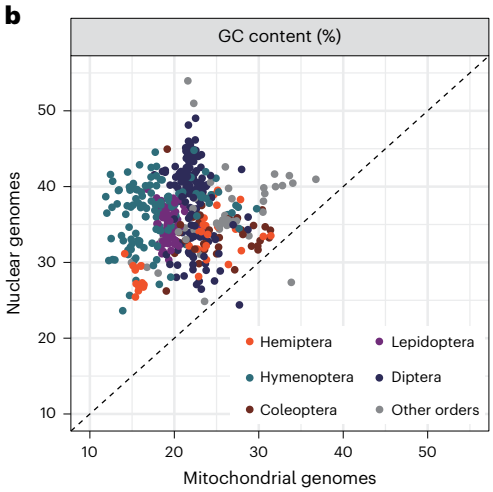

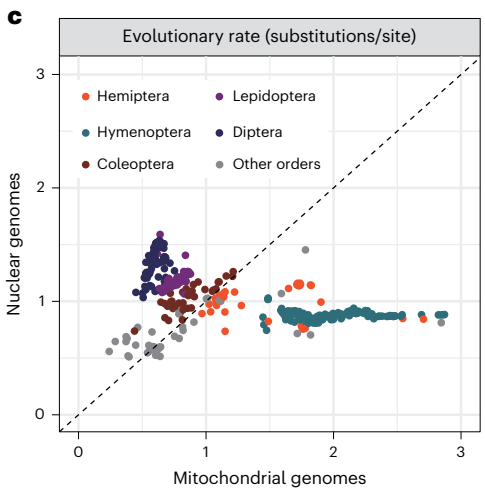

https://doi.org/10.1038/s43587-024-00641-z

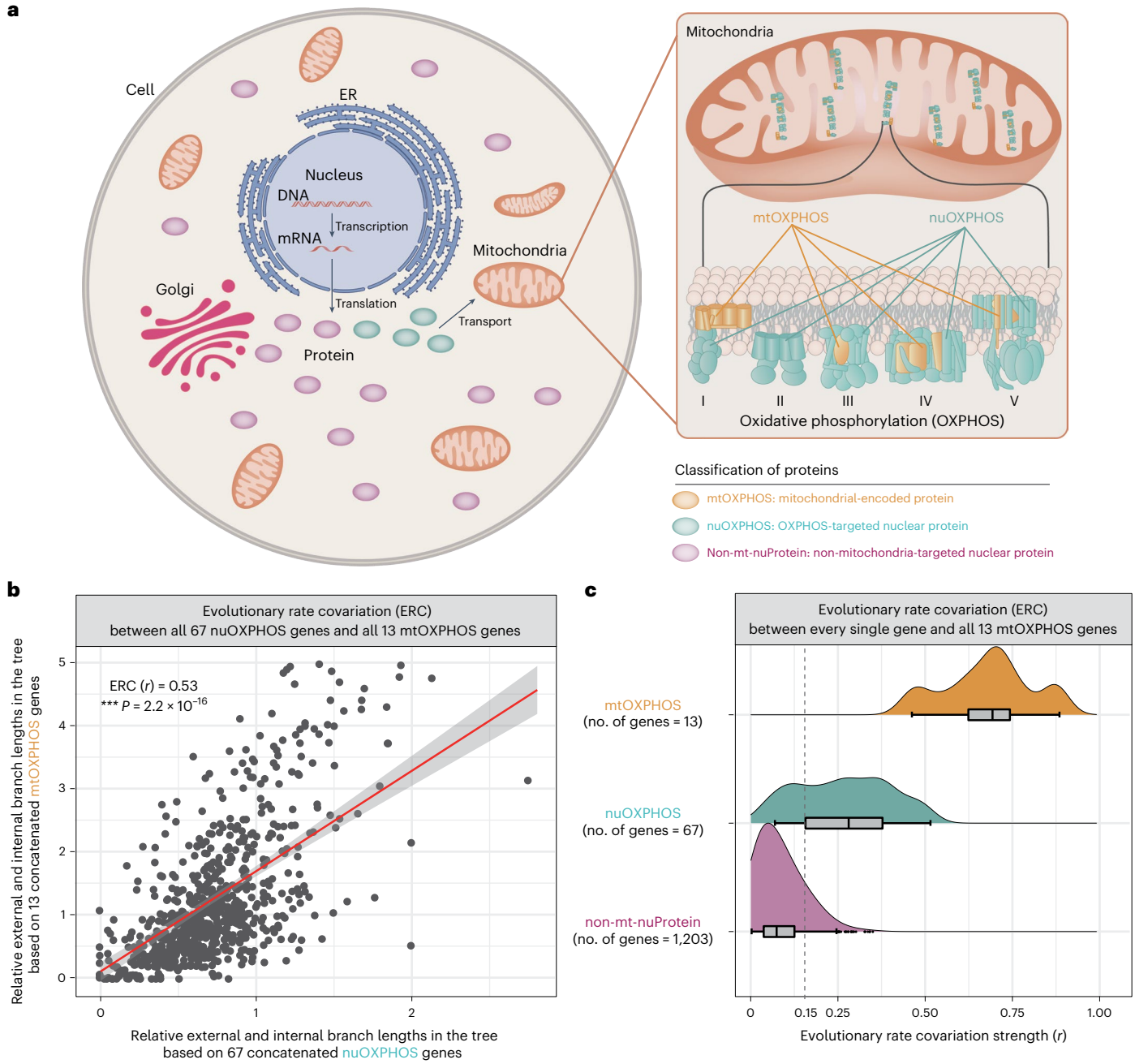

Fig. 2 | The classification of proteins and the landscape of ERC of nuclear and mitochondrial PCGs. a, The diagram of classification of proteins. Based on the subcellular locations of protein products and their involvement in the OXPHOS pathway using data from the FlyBase, we divided all 13 mitochondrial PCGs and the 1,270 nuclear protein-coding BUSCO genes into three groups: mtOXPHOS (13 mitochondrial-encoded proteins), nuOXPHOS (67 OXPHOS-targeted nuclear proteins) and non-mt-nuProtein (1,203 non-mitochondria-targeted nuclear proteins). **b**, The ERC of the nuOXPHOS supergene versus the mtOXPHOS supergene. ERC was the Pearson's correlation coefficient (r) between relative evolutionary rates estimated from each branch of the phylogeny inferred from all 67 concatenated nuOXPHOS genes (nuOXPHOS supergene) and those estimated from each branch of the phylogeny inferred from all 13 concatenated mtOXPHOS genes (mtOXPHOS supergene). Note that the nuOXPHOS supergene's phylogeny and the mtOXPHOS supergene's phylogeny were topologically identical to the reference species phylogeny of 472 insects (Fig. 1), but they exhibited different relative branch lengths across 472 insects. In addition to the ERC of the nuOXPHOS supergene versus the mtOXPHOS supergene, we also calculated the ERC of the non-mt-nuProtein supergene (which included 67 randomly concatenated non-mt-nuProtein genes) versus the mtOXPHOS supergene (Supplementary Fig. 8). Each dot in the scatter plot indicates a branch (n = 941). The red line indicates linear regression model fit, and the gray outline represents the 95% confidence interval. Two-tailed Pearson's correlation coefficient (r) was used to determine whether the two sets of values are significantly correlated. $^{***}P \leq 0.001$. **c**, The distribution of ERC values of all individual genes (13 mtOXPHOS genes, 67 nuOXPHOS genes and 1,203 non-mt-nuProtein genes) versus the mtOXPHOS supergene. For each box plot, the bottom, center and top represent 25th, 50th and 75th percentiles, respectively. Whiskers represent 1.5 × interquartile range. Outliers are data points falling above or below the ends of the whiskers. The vertical dashed gray line indicates the lower (third) quartile of the set of ERC values of all 67 nuOXPHOS genes. ER, endoplasmic reticulum.

found that correlations between nuclear and mitochondrial evolutionary rates varied among the five orders (Supplementary Fig. 7b). The underlying causes of these contrasting modes of the evolution of nuclear and mitochondrial genomes and, in particular, the surprising and striking variation in their direction among different orders remain unknown and deserve further attention.

Robust signal of ERC between nuclear and mitochondrial genes

We adopted the widely used ERC metric to identify gene–gene functional associations of nuclear and mitochondrial PCGs across 472 insects. The ERC is a Pearson's correlation coefficient (r) between relative evolutionary rates estimated from each branch of a gene's phylogeny and those of another gene's phylogeny (Extended Data Fig. 2). Because one major goal of our study is to identify nuclear PCGs that are not targeted to mitochondria but exhibit strong ERC signals and potentially interact with mtOXPHOS genes, we initially excluded 147 genes that are targeted to the mitochondria (but do not physically interact with any of the five protein complexes in the OXPHOS pathway) from the set of 1,417 conserved nuclear protein-coding BUSCO genes across 472 insects, retaining 1,270 BUSCO genes. Next, we divided all 13 mitochondrial genes and the remaining 1,270 nuclear BUSCO genes based on subcellular location and involvement in the OXPHOS pathway into three groups: mtOXPHOS (13 mitochondrial-encoded proteins), nuOXPHOS (67 OXPHOS-targeted nuclear proteins) and non-mt-nuProtein (1,203 non-mitochondria-targeted nuclear proteins) (Fig. 2a and Supplementary Table 2).

For each of three groups (mtOXPHOS, nuOXPHOS and non-mt-nuProtein), we concatenated genes into supergenes and computed ERC values. The 67 concatenated nuOXPHOS supergene exhibited strong ERC with the 13 concatenated mtOXPHOS supergene (Fig. 2b), whereas the 67 randomly concatenated non-mt-nuProtein supergene had substantially weak ERC with the 13 concatenated mtOXPHOS supergene (number of replicates = 1,000; average ERC = 0.070; 95% confidence interval: 0.058–0.082) (Supplementary Fig. 8). Additionally, we calculated the ERC value of every single gene and the 13 concatenated mtOXPHOS supergene. Individual gene ERC values varied, with mtOXPHOS genes having the highest average (0.68), followed by nuOXPHOS genes (0.27) and non-mt-nuProtein genes (0.08) (Fig. 2c and Supplementary Table 2). These results suggest that the ERC between nuOXPHOS genes and mtOXPHOS supergene was generally stronger than that between non-mt-nuProtein genes and mtOXPHOS supergene (Fig. 2c).

ERC identifies 75 mitochondria-associated nuclear genes

Our analyses showed a subset of 1,203 non-mt-nuProtein genes with similar ERC (r) values to the mtOXPHOS supergene (Fig. 2c), compared to 67 nuOXPHOS genes. To identify genes that exhibit strong ERC signals and potentially interact with mtOXPHOS genes, we initially implemented a high r threshold of ≥0.15, which is the lower (third) quartile of the set of r values of all 67 nuOXPHOS genes (Fig. 2c). This resulted in 254 genes with high r values (Fig. 3a), including 13 mtOXPHOS genes, 50 nuOXPHOS genes and 191 non-mt-nuProtein genes.

Using the 254 genes, we constructed a network based on potential protein–protein associations using the STRING database. Thirty-one clusters emerged, with the three largest (clusters 1–3) harboring 138 genes (54% of total) (Supplementary Fig. 9). Cluster 1 contained 13 mtOXPHOS genes, 50 nuOXPHOS genes and five non-mt-nuProtein genes; cluster 2 contained 50 non-mt-nuProtein genes; and cluster 3 contained 20 non-mt-nuProtein genes (Fig. 3b and Supplementary Table 3). As a result, we identified 75 non-mt-nuProteins genes showing strong ERC signals and potential functional interactions with mtOXPHOS genes. Gene Ontology (GO) enrichment analysis revealed diverse roles for these 75 non-mt-nuProtein genes, including ribosome biogenesis, DNA replication, DNA repair, telomere maintenance, metabolic process and protein localization and transport (Fig. 3c and Supplementary Table 3).

Lastly, we assessed the connectivity (that is, the number of edges connecting the examined gene to other genes) for each of the 75 non-mt-nuProtein genes in the three largest clusters 1–3 (Fig. 3b). *CG13220*, *CG11837* and *CG11788* exhibited the highest connectivity in clusters 1, 2 and 3 (Extended Data Fig. 3 and Supplementary Table 3), respectively. Based on these findings, we chose *CG13220*, *CG11837* and *CG11788* as well as *Nop60B*, which ranked as the second-highest in connectivity within the largest cluster 2 (Extended Data Fig. 3), to investigate their impact on mitochondrial morphology, following the protocol of Zhou et al.[14]. In brief, we used RNA interference (RNAi) to knock down expression with *Cg-Gal4 > UAS-mitoGFP*, which is expressed in fruit fly fat bodies and labels mitochondria with *mitoGFP*. Then, we examined the mitochondrial morphology in the early third-instar larval fat bodies using confocal microscopy. Finally, we quantified and averaged the length of mitochondria from each of five randomly selected areas (25 μm × 25 μm) within a given genotype's confocal image (four different images were examined for each genotype). Knockdown of all four tested genes led to abnormal mitochondrial morphologies (Extended Data Fig. 4a,b and Supplementary Fig. 10). Specifically, when compared to the control, knockdown of *CG13220* and *CG11788* increased mitochondrial lengths by 210% and 185% (Extended Data Fig. 4c), respectively; knockdown of *CG11837* and *Nop60B* decreased mitochondrial lengths by 48% and 59% (Extended Data Fig. 4c), respectively. These results suggest that these four non-mitochondria-targeted nuclear genes can severely affect mitochondrial morphology.

CG11837 is a conserved longevity gene

Among the 75 non-mt-nuProtein genes, we evaluated the genetic function of *CG11837*, which had a similarly high ERC value (r = 0.23) (Supplementary Table 3), the highest connectivity (Extended Data Fig. 3) and a significant impact on mitochondrial morphology in larval and adult fat body (Extended Data Fig. 4, Supplementary Fig. 11 and Supplementary Table 4). Analysis of its three-dimensional (3D) protein structure in the AlphaFold2 database[15] revealed a 93% similarity to the human *DIMT1* gene product, suggesting a role as a dimethyladenosine transferase involved in ribosome biogenesis (Extended Data Fig. 5). However, little is known about the function of *CG11837* in insects. To investigate the role of *CG11837* in *Drosophila melanogaster*, we knocked down the expression level of *CG11837* with three distinct GAL4 drivers (whole-body *Actin-GAL4*, neuronal-specific *Elav-GAL4* and motor-neuron-specific *D42-GAL4*) and assessed fly eclosion rate (Supplementary Fig. 12 and Supplementary Table 5). The choice of neuronal-specific and motor-neuron-specific drivers was based on our finding that *CG11837* can alter mitochondrial morphology (Extended Data Fig. 4 and Supplementary Fig. 11), which could potentially lead to neurodegenerative diseases and movement disorders[5]. When *CG11837* was knocked down in the whole body and neuronal cells, none of emerged flies was observed (Supplementary Fig. 12 and Supplementary Table 5). However, knockdown in motor neurons resulted in an average fly eclosion rate of 58% (Supplementary Fig. 12 and Supplementary Table 5). Therefore, we chose the *D42-GAL4 > UAS-CG11837-RNAi* line for subsequent experiments in *D. melanogaster*. In addition, we used RNAi technology with double-stranded RNA (dsRNA) injections to knock down the expression level of orthologs of *CG11837* in five other diverse organisms, including mosquito, beetle, bee, brown planthopper and worm (Extended Data Fig. 6a).

Knockdown of *CG11837* and its orthologs in fruit fly and five other diverse organisms significantly affected adult survival (Fig. 4a). To precisely quantify lifespan and reduce variation of sample sizes between treatment and control groups, we considered the timepoint by which half of the adults had died as the median lifespan for a given tested male or female species (Fig. 4a). Specifically, when compared to the genetic controls (*D42-GAL4/+* and *UAS-CG11837-RNAi/+* for fruit fly; *dsGFP* for mosquito, beetle, bee and brown planthopper; empty vector for worm), knockdowns resulted in reduced median lifespans: fruit flies (males 26–33%, females 58–59%), mosquitoes (males ~40%, females ~15%), bees (males ~40%, females ~50%) and brown planthoppers (males ~24%, females ~21%). All knockdown male and female beetles died by 24 d and 26 d, but none of control male and female adult beetles died by 30 d.

https://doi.org/10.1038/s43587-024-00641-z

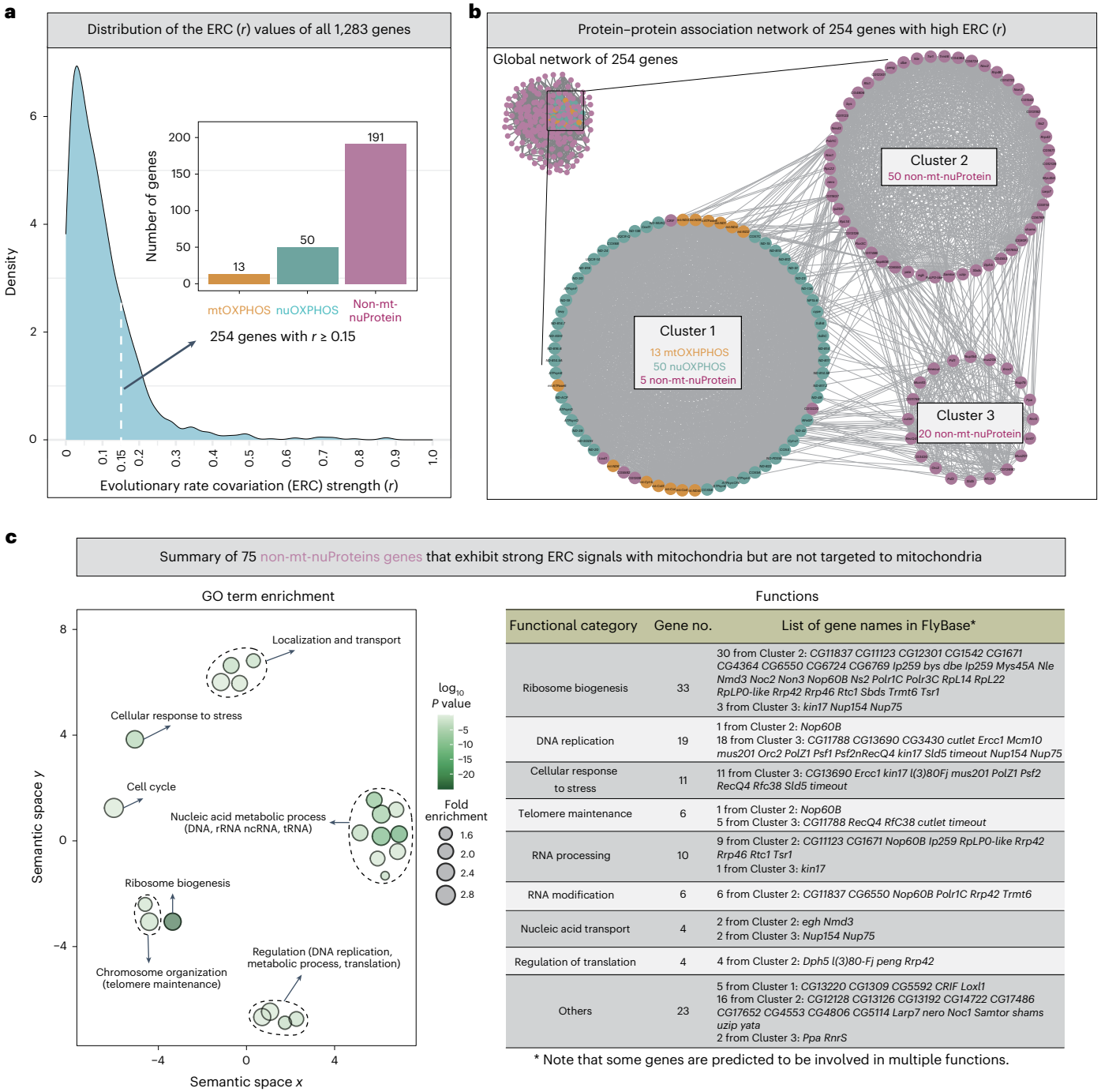

Functional category	Gene no.	List of gene names in FlyBase*
Ribosome biogenesis	33	30 from Cluster 2: *CG11837 CG11123 CG12301 CG1542 CG1671 CG4364 CG6550 CG6724 CG6769 Ip259 bys dbe Ip259 Mys45A Nle Nmd3 Noc2 Non3 Nop60B Ns2 Polr1C Polr3C RpL14 RpL22 RpLP0-like Rrp42 Rrp46 Rtc1 Sbds Trmt6 Tsr1* 3 from Cluster 3: *kin17 Nup154 Nup75*
DNA replication	19	1 from Cluster 2: *Nop60B* 18 from Cluster 3: *CG11788 CG13690 CG3430 cutlet Ercc1 Mcm10 mus201 Orc2 PolZ1 Psf1 Psf2nRecQ4 kin17 Sld5 timeout Nup154 Nup75*
Cellular response to stress	11	11 from Cluster 3: *CG13690 Ercc1 kin17 l(3)80Fj mus201 PolZ1 Psf2 RecQ4 Rfc38 Sld5 timeout*
Telomere maintenance	6	1 from Cluster 2: *Nop60B* 5 from Cluster 3: *CG11788 RecQ4 RfC38 cutlet timeout*
RNA processing	10	9 from Cluster 2: *CG11123 CG1671 Nop60B Ip259 RpLP0-like Rrp42 Rrp46 Rtc1 Tsr1* 1 from Cluster 3: *kin17*
RNA modification	6	6 from Cluster 2: *CG11837 CG6550 Nop60B Polr1C Rrp42 Trmt6*
Nucleic acid transport	4	2 from Cluster 2: *egh Nmd3* 2 from Cluster 3: *Nup154 Nup75*
Regulation of translation	4	4 from Cluster 2: *Dph5 l(3)80-Fj peng Rrp42*
Others	23	5 from Cluster 1: *CG13220 CG1309 CG5592 CRIF Loxl1* 16 from Cluster 2: *CG12128 CG13126 CG13192 CG14722 CG17486 CG17652 CG4553 CG4806 CG5114 Larp7 nero Noc1 Samtor shams uzip yata* 2 from Cluster 3: *Ppa RnrS*

* Note that some genes are predicted to be involved in multiple functions.

Fig. 3 | Identification of non-mitochondria-targeted nuclear genes that exhibit strong ERC and potentially interact with mtOXPHOS genes. a, The distribution of ERC values between all 1,283 individual genes (13 mtOXPHOS genes, 67 nuOXPHOS genes and 1,203 non-mt-nuProtein genes) and the mtOXPHOS supergene. To identify non-mitochondria-targeted nuclear genes that exhibit strong ERC and potentially interact with mtOXPHOS genes, an ERC (*r*) threshold of ≥0.15, which was the lower (third) quartile of the set of ERC values of all 67 nuOXPHOS genes (Fig. 2c), was used to initially retain 254 genes, including 13 mtOXPHOS genes, 50 nuOXPHOS genes and 191 non-mt-nuProtein genes. **b**, The analysis of protein–protein association network of the 254 genes with high *r* values. In total, 254 genes were grouped into 31 clusters, each of which consists of at least two genes (Supplementary Fig. 9). Among 31 clusters, the three largest clusters contained 138 (cluster 1: 68; cluster 2: 50; cluster 3: 20) out of 254 (54%) genes, whereas the remaining 28 small clusters included 2–6 genes each. This analysis resulted in 75 non-mitochondria-targeted nuclear genes (cluster 1: 5; cluster 2: 50; cluster 3: 20) that exhibit strong signals of ERC with the mitochondria and potentially interact with them. Furthermore, we investigated the connectivity (that is, the number of edges connecting the examined gene to other genes in the three largest clusters) for each of the 75 non-mt-nuProtein genes (Extended Data Fig. 3). **c**, GO enrichment analysis (left) and functional categories (right) of 75 non-mitochondria-targeted nuclear genes. ncRNA, non-coding RNA; tRNA, transfer RNA.

Knockdown in worms, being hermaphrodites, had approximately 33% decrease in median lifespan compared to the controls.

To assess the impact of overexpression at different developmental stages on adult lifespan (Extended Data Fig. 6b), *E02H1.1* was overexpressed throughout the worm life cycle, whereas *CG11837* in fruit fly was overexpressed only in adults using a temperature-sensitive transgenic line (*Actin-GAL4 tsGAL80 > UAS-CG11837*) at 29 °C. Compared to two genetic controls (*Actin-GAL4 tsGAL80/+* and *UAS-CG11837/+*),

CG11837 overexpression extended median lifespans by 30–59% in male flies and by 27–30% in female flies (Fig. 4b). Additionally, *E02H1.1* overexpression in worms (being hermaphrodites) increased median lifespan by 12% (Fig. 4b) compared to control worms.

We also overexpressed the human gene *DIMT1*, an ortholog of *CG11837*, in human skin fibroblast HCA2 cells. Under standard conditions, *DIMT1*-overexpressing and control cells showed similarly low levels of senescence-associated β-galactosidase (SA-β-gal) activity, a marker of cell senescence (overexpression: 2.4%; control: 2.4%) and high cell proliferation capability (overexpression: 96.3%; control: 97.2%) (Fig. 4c, Extended Data Fig. 7, Supplementary Fig. 13 and Supplementary Table 6). However, upon exposure to X-ray irradiation (IR), *DIMT1*-overexpressing cells displayed an approximately 30% reduction in SA-β-gal activity (overexpression: 64.8%; control: 92.1%) and a 2.8-fold increase in cell proliferation (overexpression: 23.7%; control: 6.3%) (Fig. 4c, Extended Data Fig. 7, Supplementary Fig. 13 and Supplementary Table 6).

Given the increased lifespan with *CG11837* overexpression, we analyzed the correlation between *CG11837* gene expression levels and lifespans from 43 insects representing nine orders (Supplementary Table 7). We found that relative expression levels of *CG11837* in 43 insects were significantly positively correlated ($r = 0.45$, $P = 0.002$) with their lifespans (Supplementary Fig. 14a and Supplementary Table 7). Additionally, we examined *DIMT1* in BXD mouse strains[16] and found a significant positive correlation ($r = 0.58$, $P = 0.0058$) between the lifespans of BXD strains and *DIMT1* expression levels (Supplementary Fig. 14b and Supplementary Table 8).

To further explore what pathway(s) are associated with the lifespan-associated gene *CG11837*, we conducted whole-body transcriptome analyses on *CG11837* knockdown versus control male mosquitoes and beetles as well as *CG11837* overexpression versus control male adult fruit flies (Methods). KEGG pathway enrichment analysis revealed that the genes significantly downregulated in *CG11837* knockdown mosquitos and beetles, as well as those significantly upregulated in *CG11837* overexpression fruit flies, are mainly involved in energy-related pathways, such as OXPHOS and carbon metabolism (Extended Data Fig. 8). Surprisingly, out of 80 OXPHOS genes (13 mtOXPHOS genes and 67 nuOXPHOS genes), 63 and 71 genes were expressed at lower levels in *CG11837* knockdown mosquitos and beetles, respectively (Fig. 4d and Extended Data Fig. 8a). Conversely, *CG11837* overexpression fruit flies increased expression of 73 out of 80 OXPHOS genes (Fig. 4d and Extended Data Fig. 8b). Furthermore, comparing expression levels of all 80 OXPHOS genes between young and aged wild-type diverse insects[17–21] revealed a decrease in OXPHOS gene expression with age (Extended Data Fig. 9). Given that OXPHOS plays a central role in cellular energy synthesis, we examined ATP production and found that *CG11837* knockdown male mosquitos significantly reduced ATP production (Fig. 4e). Conversely, overexpression of *CG11837* in male fruit flies significantly increased ATP production (Fig. 4e). Collectively, these results suggest that increased activity of *CG11837* may potentially extend lifespan by enhancing the OXPHOS pathway.

Discussion

Many studies have demonstrated the utility of ERC in identifying gene–gene functional associations[7–9,22,23]. In our investigation of 472 insects, we observed strong ERC between nuOXPHOS and mtOXPHOS genes (Fig. 2b). Most of the 1,203 non-mitochondria-targeted nuclear genes showed lower ERC values with mtOXPHOS genes compared to nuOXPHOS genes (Fig. 2c), likely due to divergent evolutionary modes of nuclear and mitochondrial genomes (Fig. 1). To mitigate false positives, we performed functional protein–protein association network analyses based on 254 genes with an ERC value of ≥0.15 (Fig. 3a,b), identifying 75 non-mt-nuProteins candidate genes with diverse functions (Fig. 3c). Knocking down four of these candidate genes in fruit fly larval fat body severely affected mitochondrial morphology (Extended Data Fig. 4). These findings underscore ERC's potency in pinpointing genes with shared functions, offering potential insights into aging-related signaling pathways, such as insulin, mTOR or sirtuin signaling. This potential would be strengthened by leveraging aging-related resources, such as genome-wide association study data[24], single-cell transcriptome data[25] and epigenomic data[26].

The OXPHOS pathway, vital for cellular energy synthesis, relies on both mtOXPHOS and nuOXPHOS PCGs in most animals. Dysfunction of mtOXPHOS and nuOXPHOS genes can lead to a variety of disorders, such as aging-related diseases[4], neurodegenerative diseases[5] and metabolic disorders[6]. Our study functionally validated a non-mitochondria-targeted nuclear gene, *CG11837*, which is conserved across animals, and exhibited strong ERC with mtOXPHOS genes and severely affected mitochondrial morphology. Knockdown of *CG11837* shortened lifespans in six diverse organisms, and overexpression increased lifespan in fruit fly and worm (Fig. 4a,b). Furthermore, *DIMT1* (an ortholog of *CG11837*) overexpression in human cells reduced cellular senescence and rescued cell proliferation arrests in response to DNA damage (Fig. 4c, Extended Data Fig. 7 and Supplementary Fig. 13). Elevated *CG11837* activity increased nearly all OXPHOS gene expressions (Fig. 4d). Many longevity-promoting genes have been reported across species from fungi to mammals. For example, *Sir2*, a member of the Sirtuin family, has been reported to promote longevity in yeast. However, studies on the effects of *Sir2* on lifespan extension in worms and flies have yielded conflicting results[27–29]. In our study, we identified a longevity gene, *CG11837*, that plays a significant role in extending lifespan, observed from worm to insect, and, potentially, this effect could extend to mammals, including humans. Although the mechanism underlying the extension of lifespan by *CG11837* in insects remains unclear, previous studies indicated that its ortholog *DIMT1*

Fig. 4 | *CG11837* is a conserved lifespan gene across animals. a, Effect of knockdown of *CG11837* and its orthologs on adult survival rates of six diverse organisms. Median lifespans for males (solid) and females (dashed) in control and knockdown groups are provided with temperatures. Fruit fly used two genetic controls (*D42-GAL4/+* and *UAS-CG11837-RNAi/+*); mosquito, beetle, bee and brown planthopper used *dsGFP* as controls; worm used empty vector as a control. Each experiment was conducted with three biological replicates. *P* values were determined by two-sided log-rank test. $^{**}P \le 0.01$ and $^{***}P \le 0.001$. **b**, Effect of overexpression of *CG11837* and its ortholog on survival rates of fruit fly (*Actin-GAL4 tsGAL80 > UAS-CG11837*) and worm ($E02H1.1^{OE}$), respectively. Median lifespans for male (solid) and female (dashed) fruit flies in control and treatment groups are provided with temperatures. Fruit fly used two genetic controls (*Actin-GAL4 tsGAL80/+* and *UAS-CG11837/+*); worm used N2 Bristol strain as a control. We conducted three biological replicates for each experiment. *P* values were determined by two-sided log-rank test. $^{***}P \le 0.001$. Worms are hermaphrodites. **c**, *DIMT1* overexpression in HCA2 cells, control (empty vector) versus DIMT1-overexpressing, with or without 5 Gy X-ray, quantified for SA-β-gal, a biomarker of senescent cell. Three biological replicates were conducted for each experiment. Data represent mean ± s.d. *P* values were calculated using two-tailed *t*-test. NS $P > 0.05$ and $^{***}P \le 0.001$. **d**, Comparison of OXPHOS expression levels in control versus *CG11837* knockdown 3-day-old male adult mosquitos (left) and in control versus *CG11837* overexpression 3-day-old male adult fruit flies (right). For each box plot (sample size = 80), bottom, center and top represent 25th, 50th and 75th percentiles, respectively. Whiskers represent 1.5 × interquartile range. *P* values were calculated using the two-tailed paired Wilcoxon test. $^{***}P \le 0.001$. **e**, Comparison of ATP production in control versus *CG11837* knockdown 3-day-old male adult mosquitos (left) and in control versus *CG11837* overexpression 3-day-old male adult fruit flies (right). Three biological replicates were conducted for each experiment. Data represent mean ± s.d. *P* values were calculated using two-tailed *t*-test. $^{**}P \le 0.01$. All images were taken from the free-to-use PhyloPic website (http://phylopic.org)[58]. TPM, transcripts per million.

https://doi.org/10.1038/s43587-024-00641-z

is involved in ribosome assembly and protein translation fidelity in human cell lines[30–32]. Additionally, a recent study found that *DIMT1* is necessary for the transmission of intergenerational hormesis by catalyzing ribosomal RNA (rRNA) methylation in response to starvation in worm[33]. Given these previous findings and the predicted function of *CG11837* as a dimethyladenosine transferase, exploring how

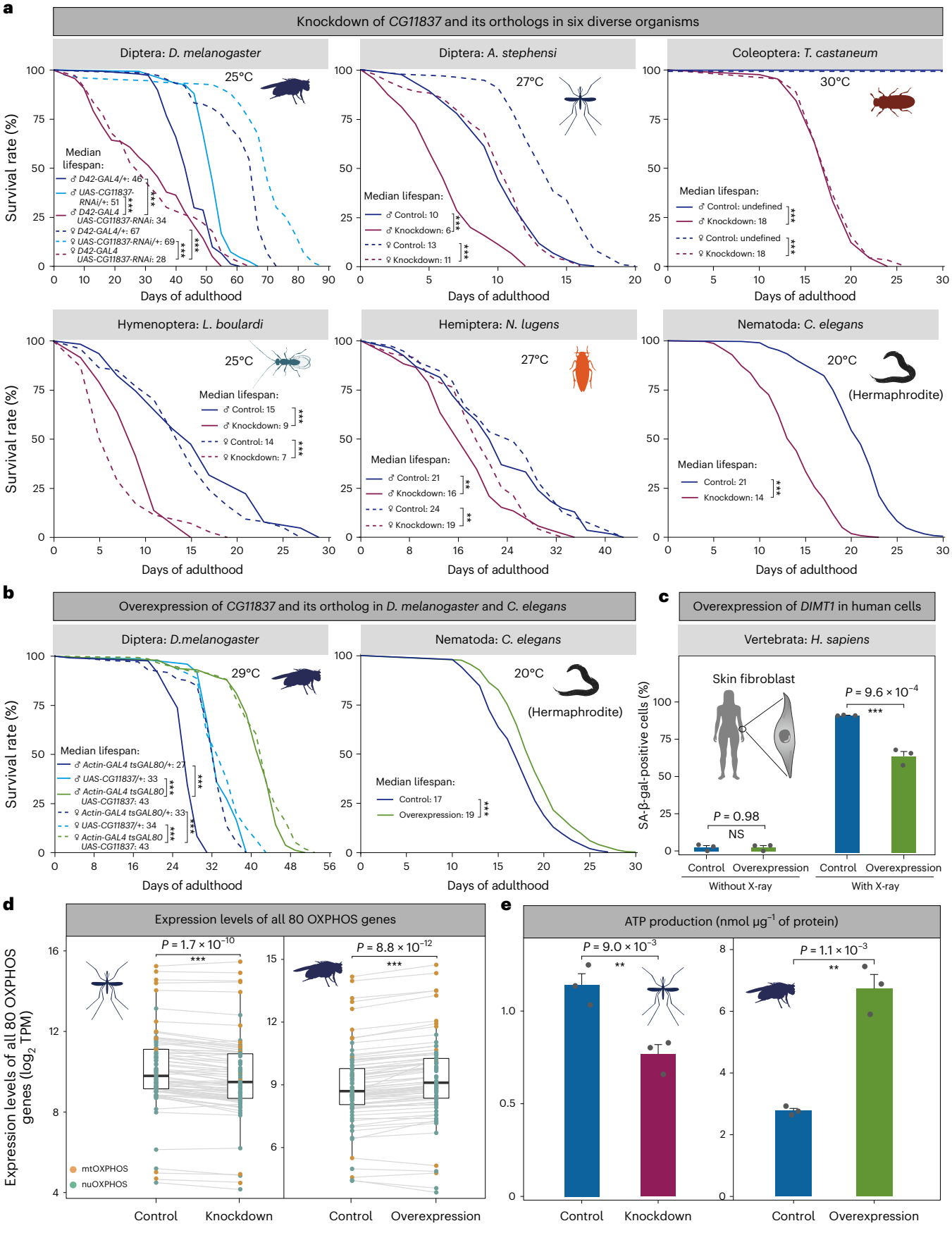

CG11837/*DIMT1* contributes to longevity across animals is an exciting future direction, particularly in the field of epigenetics.

Our study focused primarily on nuclear PCGs not targeted to mitochondria but displaying strong ERC with mtOXPHOS genes. However, nuOXPHOS genes also play a crucial role in cellular energy harvesting. For instance, investigating copper resistance variation among wild fruit fly populations, Everman et al.[34] identified copper-associated single-nucleotide polymorphisms (SNPs) in certain nuOXPHOS genes, including bellwether (*blw*). Excessive copper exposure was found to impact the expression levels of nuOXPHOS genes in fruit flies, causing decreased ATP production[35] and higher levels of reactive oxygen species (ROS)[36]. Furthermore, our study centered primarily on the set of 1,417 conserved nuclear BUSCO genes, which represent only a fraction of the nuclear genome encoding tens of thousands of genes. Therefore, investigations into the ERC between mitochondrial and nuclear genomes using all nuclear genes and all OXPHOS genes (mtOXPHOS and nuOXPHOS genes) represent promising directions for future research and could offer additional insights into the interplay between these two genomes.

Methods

Taxon sampling

Nuclear genomes. To collect the greatest possible set of the full genome representatives of the class Insecta as of 9 May 2020, we used 'insects' as a search term in the National Center for Biotechnology Information (NCBI) Genome browser to obtain the basic information of species name, assembly accession number, assembly release date, assembly level and GenBank FTP access number. Collectively, we sampled 472 insect genomes (Supplementary Table 1). To assess quality of genome assemblies, we ran BUSCO version 5.2.2 (ref. 37) with the genome mode option ('-m genome'). Each assembly's completeness was evaluated using 1,417 full-length BUSCO nuclear genes from 75 insect genomes in the OrthoDB version 10 database. For each BUSCO gene, its consensus orthologous protein sequence among the reference genomes was queried using tBLASTn against each assembly, identifying up to three putative genomic regions. Gene structure prediction was performed using MetaEuk version 5-34c21f2 (ref. 38). Predicted genes were aligned to the hidden Markov model (HMM) profile of the BUSCO gene. BUSCO genes were classified as 'single-copy, full-length' if one complete gene was present, as 'duplicated, full-length' if two or more complete genes were present, as 'fragmented' if gene length was less than 95% of the reference and as 'missing' if no gene was predicted. Here, we considered single-copy, full-length genes and duplicated, full-length genes as complete genes. To construct the phylogenetic data matrix, we started with the set of 1,417 single-copy, full-length BUSCO genes from 472 insect genomes. For each BUSCO gene, we used BUSCO output table 'full_table.tsv' to collate single-copy, full-length amino acid sequences from BUSCO output folder 'single_copy_busco_sequences' across all genomes into a single FASTA file. These 1,417 BUSCO genes were used for phylogenetic analyses and ERC analyses.

Mitochondrial genomes. For 237 insects lacking mitochondrial genomes, we retrieved approximately 2–3 million raw reads from the whole-genome sequencing (WGS) data in the NCBI's Sequence Read Archive browser to assemble mitochondrial genomes using GetOrganelle version 1.7.3.5 (ref. 39). We used MitoZ version 2.3 (ref. 40) to annotate the mitochondrial genome. The completeness of the mitochondrial genome was gauged by assessing the occupancy of all 13 PCGs.

Phylogenetic analyses

To infer two genome-scale phylogenies of 472 insects for nuclear genomes and mitochondrial genomes, we included 15 outgroups from Entognatha.

A genome-scale phylogeny of 472 insects using nuclear genomes. For each of 1,417 nuBUSCO genes, amino acid sequences were aligned using MAFFT version 7.299b (ref. 41) with the options '–thread 12–auto–maxiterate 1000' and trimmed using trimAl version 1.4.rev15 (ref. 42) with the options '-gappyout -colnumbering'. We inferred concatenation-based ML tree using IQ-TREE multicore version 1.6.8 (ref. 43) under a single 'LG + G4' model with the options '-nt 50 -mem 350 G -m LG + G4 -bb 1000'. Five independent tree searches were conducted.

A genome-scale phylogeny of 472 insects using mitochondrial genomes. Each of 13 mtPCGs underwent multiple amino acid sequence alignments and trimming of ambiguously aligned regions, following the same procedure described above for the nuBUSCO data matrix. We inferred tmtPCG concatenation-based ML tree using IQ-TREE under a single 'mtInv+F + G4' model with the options '-nt 20 -mem 10 G -m mtInv+F + G4 -bb 1000'. Five independent tree searches were conducted.

ERC calculations

Dataset. Before ERC calculation, we excluded 147 nuclear BUSCO genes targeted to mitochondria without interacting with OXPHOS pathway proteins. Using the FlyBase database (https://flybase.org/), we categorized 13 mitochondrial and 1,270 nuclear BUSCO genes into three groups: mtOXPHOS (13 mitochondrial-encoded proteins), nuOXPHOS (67 OXPHOS-targeted nuclear proteins) and non-mt-nuProtein (1,203 non-mitochondria-targeted nuclear proteins).

Workflow of ERC calculation. In brief, to account for evolutionary rates and independent branch length contrasts, we transformed branch lengths into relative evolutionary rates by dividing gene tree branch length by background branch length in the reference species phylogeny inferred from all nuclear genes. Subsequently, we calculated the Pearson's correlation coefficient (r) of the relative evolutionary rates between a given gene and the mtOXPHOS supergene (13 concatenated mtOXPHOS genes) using a three-step workflow (Extended Data Fig. 2) following Steenwyk et al.[22].

In step 1, we estimated all branch lengths for a given gene and the mtOXPHOS supergene based on the topology of the reference species tree (Fig. 1a)—namely, the nuBUSCO phylogeny that was largely congruent with a previous genome-scale phylogeny of 103 insects[13].

In step 2, we normalized the re-estimated branch lengths for a given gene and the mtOXPHOS supergene to the relative evolutionary rates by dividing the branch lengths of the gene tree by those of the reference species tree.

In step 3, we calculated the Pearson's correlation coefficient (r) between relative evolutionary rates estimated from a given gene and those estimated from the mtOXPHOS supergene as the ERC value.

ERC of nuOXPHOS supergene and non-mt-nuProtein supergene with mtOXPHOS supergene. For nuOXPHOS supergene, we concatenated all 67 individual genes into a supergene. For non-mt-nuProtein supergene, we randomly concatenated 67 non-mt-nuProtein genes (by sampling genes with replacement) from the set of 1,203 non-mt-nuProtein genes into a supergene. This procedure was repeated 1,000 times. For a given supergene, we calculated its ERC with the mtOXPHOS supergene, using the above workflow.

ERC of every single gene and mtOXPHOS supergene. For each of all 1,290 genes (13 mtOXPHOS genes, 67 nuOXPHOS genes and 1,203 non-mt-nuProtein genes), we calculated its ERC with the mtOXPHOS supergene, using the above workflow. Note that the reference species tree was pruned to match the taxon set in single-gene alignment if the reference species tree contained taxa that were absent from the single-gene alignment.

ERC of every single gene and mtRNA supergene. In addition to 13 mtOXPHOS genes, bilaterian mitochondrial genomes also typically contain 24 non-coding RNA genes (24 mtRNA genes)[44]. We also used 24 mtRNA genes as targets to investigate ERC for all 1,290 genes (13 mtOXPHOS genes, 67 nuOXPHOS genes and 1,203 non-mt-nuProtein genes). We found that the 24 concatenated mtRNA supergene exhibited a significantly strong signal of ERC with the 13 concatenated mtOXPHOS

supergene (ERC value = 0.89, $P = 2.2 \times 10^{-16}$) (Supplementary Fig. 15a). Furthermore, we identified 196 individual genes that displayed a strong ERC with the mtRNA supergene (Supplementary Fig. 15b). Among these 196 genes, 129 genes (66%) were also present in the list of 254 genes showing a strong ERC with the mtOXPHOS supergene. These findings imply a highly similar mode of evolution between mtOXPHOS genes and mtRNA genes in mitochondria.

Identification of mitochondria-associated nuclear genes

To identify non-mitochondria-targeted nuclear genes that display strong ERC with the OXPHOS genes and functionally associated with the mitochondria, we applied 254 genes with an ERC (r) threshold of ≥0.15 (Fig. 2c) to construct a protein–protein association network using the STRING database[45]; default parameters were used. The protein–protein association network was visualized using Cytoscape version 3.9.0 (ref. 46). These 254 genes were grouped into 31 clusters, each of which contains at least two genes (Supplementary Fig. 9). Here, we focused on the three largest clusters 1–3, which consist of 5, 50 and 20 non-mitochondria-targeted nuclear genes, respectively. Furthermore, we assessed the connectivity (that is, the number of edges connecting the examined gene to other genes) for each of the 75 non-mt-nuProtein genes in the clusters 1–3. To investigate the functions of these 75 genes, we carried out GO enrichment analysis using Metascape version 3.5 (ref. 47). The significantly enriched GO terms were summarized and visualized using REVIGO version 20150217beta (ref. 48).

Effect of RNAi of four candidate genes on mitochondria

We knocked down expression of *CG13220*, *CG11837*, *CG11788* and *Nop60B* in fat body using *UASRNAi* lines and *CgGal4* following the protocol of Zhou et al.[14]. *D. melanogaster UAS-CG11837-RNAi* (THU5456) line was acquired from the TsingHua Fly Center; this line corresponds to the HMS02625 from the TRiP RNAi library and is also available in the Bloomington Drosophila Stock Center (BDSC_42932). *UAS-CG13220-RNAi* (HMJ21671; BDSC_52984), *UAS-CG11788-RNAi* (HMJ21486; BDSC_54043) and *UAS-Nop60B-RNAi* (HMC04815; BDSC_57500) lines were acquired from the Bloomington Drosophila Stock Center. The reporter line *Cg-GAL4 > UAS-mitoGFP* was provided by Chao Tong (Zhejiang University).

The early third-instar larval fat bodies were dissected in 1× PBS and fixed with 4% paraformaldehyde for half an hour. The mitochondria in each sample were marked with mitoGFP and examined without antibody immunostaining. Samples were rinsed three times with 1× PBST (PBS containing 0.1% Triton X-100 and 0.05% Tween 20) and then mounted in ProLong Gold Antifade Mountant with blue fluorescent DNA stain DAPI (Invitrogen). All the samples were imaged by using a ×63/1.4 NA oil immersion lens with a Zeiss LSM 800 confocal microscope. Additionally, we verified the presence of lipid droplets in the genetic background fly *Cg-GAL4 > UAS-mitoGFP* with 1× PBS of 0.05% Nile Red (Sigma-Aldrich, 19123) at a final dilution of 1:2,000. For a given confocal image, we measured and averaged the length of mitochondria from each of five randomly selected areas (25 µm × 25 µm). The quantification of mitochondrial length was performed with four different images. Given that *CG11837* can affect the adult lifespan in diverse organisms (Fig. 4), we also examined the effect of knocking down *CG11837* on mitochondrial morphology for the 3-day-old adult fat body (Supplementary Fig. 11) and found that knockdown of *CG11837* also led to abnormal mitochondrial morphology in adult fat body, consistent with the finding in the early third-instar larval fat body (Extended Data Fig. 4).

Knockdown of *CG11837* and its orthologs in diverse organisms

We used RNAi to knock down the expression levels of *CG11837* in fruit fly and its orthologs in five diverse organisms: *LOC118508549* in mosquito *Anopheles stephensi*, *LOC661358* in beetle *Tribolium castaneum*, *LOC127283745* in bee *Leptopilina boulardi*, *LOC111053781* in brown planthopper *Nilaparvata lugens* and *E02H1.1* in worm *C. elegans*.

Detailed information of all animal rearing and the RNAi assay is given in the Supplementary Methods and in Supplementary Tables 9–11. For each examined species, we amplified the target gene using cDNA by polymerase chain reaction (PCR) with primers containing the T7 primer sequence at the 5′ ends and then sequenced the PCR products using Sanger sequencing. Next, we used PCR products as templates to synthesize the dsRNA using a MEGAscript RNAi Kit (Life Technologies) and measured the concentration of dsRNAs by NanoDrop 2000 (Thermo Fisher Scientific). Third, female and male adults (except for hermaphrodite worms) were injected with dsRNAs by micro-injection, respectively. The efficiency of RNAi in 3-day-old adult whole body was determined by quantitative real-time PCR (qPCR), unless otherwise indicated. Overall, the efficiencies of knocking down expression levels of *CG11837* and its orthologs by RNAi vary between 43% and 97%. The lifespan assays were performed in three replicates on both sexes (except for hermaphrodite worms). Each replicate was at least 20 individuals. *dsGFP* was synthesized and used as a negative control, unless otherwise indicated.

Overexpression of *CG11837* in fruit fly and worm

To assess the impact of *CG11837* overexpression at different developmental stages on adult lifespan, we overexpressed *CG11837* only at adult stage, whereas *E02H1.1* in worm was overexpressed throughout the entire life cycle.

To generate the transgenic flies that overexpressed *CG11837* throughout whole body at the adult stage, we used a temperature-sensitive conditional *GAL4/GAL80ts* system to drive *UAS-CG11837* expression only in adults. Flies were raised at 18 °C to suppress *GAL4* activity during developmental stages. After eclosion, the adults were switched to 29 °C to inactivate *GAL80ts* and, thereby, permit *GAL4* activation of *UAS-CG11837*. The *tub-GAL80^{ts}* (tsGAL80) and *Actin-GAL4* lines were from the Daniel Kalderon laboratory (Columbia University). For *UAS-CG11837* transgenic flies, we amplified the coding region of *CG11837* from cDNA of *Drosophila W^{1118}* strain. Then, the resulting cDNA fragment was inserted into the *pUAST-attB* vector digested with Kpn-I. The plasmid of *CG11837* was injected into *Drosophila* embryos and specifically integrated into the *attP* site on chromosome 2 (attP2, 25C6). Eclosed virgin male and female adults of each genotype were collected and kept separately at a density of approximately 50 flies per bottle at 29 °C and 50% relative humidity under a 16-h light and 8-h dark photoperiod. The flies were transferred to fresh medium every 2–3 d, and the number of dead flies was recorded until all flies died. The efficiencies of 3-day-old overexpression male and female adult whole bodies were 59.6-fold and 4.8-fold, respectively.

For overexpression of *E02H1.1* in hermaphrodite *C. elegans* worms, overexpressed *E02H1.1* was driven by its own promoter through the entire worm life cycle. Specifically, *C. elegans* were cultured on nematode growth medium (NGM) plates with *Escherichia coli* OP50 at 20 °C. The N2 Bristol strain was used as the control strain. Standard procedures were used to construct overexpression strains using the CRISPR–Cas9 genome editing method, and these strains were genotyped by PCR and sequencing. Standard microinjection methods were used to generate transgenic animals carrying extrachromosomal arrays (*zjuEx*). For extrachromosomal array transgenic worms (P*E02H1.1*-E02H1.1 [*zjuEx2441*]), 10 ng µl^{-1} plasmids and 50 ng µl^{-1} co-injection marker (*Pttx-3-RFP*) were injected into N2 animals. L4 stage worms were picked onto 6-cm NGM plates. Worms that escaped or died by bursting through the vulva were censored. Survival was scored daily. The transgenic worms (P*E02H1.1*-E02H1.1 [*zjuEx2441*]) had approximately 2.2-fold higher expression level of *E02H1.1* than the control trains.

Overexpression of *DIMT1* in human cells

Cell line. Human primary skin fibroblast HCA2 cells were obtained from the Huffington Center on Aging and named by Olivia Pereira-Smith. The cells were immortalized by overexpressing a human telomerase

(hTERT). Cells were cultured in EMEM media (American Type Culture Collection) containing 15% (v/v) FBS and 1% (v/v) penicillin–streptomycin and maintained in a 37 °C incubator in an atmosphere of 5% CO_2 and 3% O_2.

Plasmids and transfection. The coding sequence (CDS) of human *DIMT1* (an ortholog of *CG11837*) was cloned into a modified piggyBac (pPB) expression vector. Growing human fibroblasts were harvested and transfected with 5 µg of pPB and 5 µg of pPB transposase (pBase) plasmids per 1×10^6 cells using a Lonza Nucleofector II machine, with program T-020 and NHDF solution (Amaxa). Cells were selected with puromycin, and survived cells were collected and pooled for downstream experiments.

Western blot. Cells were lysed with 2 × Laemmli buffer (Bio-Rad) containing protease inhibitor cocktail (Roche) and boiled. The protein samples were resolved by SDS-PAGE and transferred to a PVDF membrane (Bio-Rad). The membranes were blocked with 5% non-fat milk in TBS containing 0.1% Tween 20 (TBS-T), followed by incubation with primary antibody against DIMT1 (Abcam, ab271003) or β-actin at 4 °C overnight. Membranes were incubated with HRP-conjugated anti-rabbit IgG secondary antibody (Abcam) at room temperature for 1 h. Proteins were visualized on a gel imager (Bio-Rad) using an ECL kit (Zen-Bio).

Senescence induction by X-ray. Growing human fibroblasts were subjected to 5 Gy X-ray IR and allowed to grow for 10 d for SA-β-gal or 2 d for 5′-bromo-2′-deoxyuridine (BrdU) assay.

SA-β-gal assay. Ten days after IR, cells were trypsinized and seeded in six-well plates in low density. Twenty-four hours later, cells were fixed with 2% formaldehyde and 0.2% glutaraldehyde in PBS for 5 min at room temperature. Cells were stained with a staining solution containing 20 mg ml^{-1} X-gal in dimethylformamide, 0.2 M citric acid/Na phosphate buffer (pH 6.0), 100 mM potassium ferrocyanide, 100 mM potassium ferricyanide, 5 M $NaCl_2$ and 1 M $MgCl_2$. The plates were incubated at 37 °C for 16 h without CO_2. Images of three different areas from three different samples were captured, and SA-β-gal staining of at least 50 cells in each area was counted.

BrdU incorporation assay. Two days after IR, cells were incubated with BrdU (3 µg ml^{-1}) for 48 h. The cells were then fixed using 4% paraformaldehyde for 30 min and washed with PBS five times, followed by treatment with 2 N HCl for 30 min. Cells were blocked for 2 h using 5% FBS in PBS with 0.2% Triton X-100. A FITC-conjugated anti-BrdU antibody (Thermo Fisher Scientific, 1:200) was used to incubate the cells at 4 °C overnight. Cells were mounted with DAPI Fluoromount-G for 10 min and then observed under a fluorescence microscope. Images were acquired by scanning the whole slide, and three random areas from three different samples were picked for quantification.

Transcriptome

RNA sequencing. Total RNA from *CG11837* knockdown and control male adults of 3-day-old *A. stephensi*, 13-day-old *T. castaneum* and *CG11837* overexpression and control male adults of 3-day-old *D. melanogaster* was isolated using a FastPure Cell/Tissue Total RNA Isolation Kit (Vazyme). Residual DNA was removed per the manufacturer's protocol. RNA sequencing libraries were constructed and sequenced on an Illumina HiSeq 2000 (paired ends).

Transcriptome analysis. Trimmomatic version 0.39 (ref. 49) removed low-quality reads and adapter sequences. Clean reads were mapped to the reference genome using STAR version 2.7.10a (ref. 50), and featureCounts version 2.0.1 (ref. 51) counted reads per gene. DESeq2 version 1.30.1 (ref. 52) analyzed differential expression, considering genes with adjusted $P \leq 0.05$ and $|\log2 \text{fold change}| \geq 1$. KEGG enrichment analysis was conducted using ShinyGO 0.77 (ref. 53).

ATP production assay

ATP production levels were detected using an ATP assay kit (Beyotime Biotechnology) following the manufacturer's instructions. We quantified ATP production for *CG11837* knockdown and control 3-day-old adult male *A. stephensi* as well as *CG11837* overexpression and control 3-day-old adult male *D. melanogaster*, respectively. In brief, three adult males for each genotype were lysed in ATP lysis buffer and centrifuged at 12,000*g* for 5 min at 4 °C. A 20-µl aliquot of supernatant from each sample was incubated with 100 µl of ATP working buffer, and the ATP levels were measured using a SpectraMax iD5 Multi-Mode Microplate Reader (Molecular Devices). The values were normalized to the amount of total protein in each sample, which was determined using a BCA Protein Assay Kit (Invitrogen). The measurements were repeated three times for each species.

Statistics and reproducibility

All statistical analyses were performed in R version 3.4.2. Experiments were performed with three or more biological replicates. Data are shown as the mean ± s.d. Comparisons were conducted using two-tailed Student's *t*-test or two-tailed paired Wilcoxon test as indicated in the figure legends. Additionally, correlation analyses were conducted using two-tailed Pearson's correlation method. Significance throughout the paper is designated as follows: not significant (NS) > 0.05; $^*P \leq 0.05$; $^{**}P \leq 0.01$; and $^{***}P \leq 0.001$. Data distribution was assumed to be normal, but this was not formally tested. No randomization method was used to allocate samples to experimental groups. Data collection and analysis were not performed blinded to the conditions of the experiments. No data were excluded from the analyses.

Reporting summary

Further information on research design is available in the Nature Portfolio Reporting Summary linked to this article.

Data availability

All mitochondrial genomes, phylogenomic matrix, gene trees and summary statistics as well as 3D protein structures of 75 non-mitochondria-targeted nuclear proteins are available on the figshare repository (https://doi.org/10.6084/m9.figshare.22637761)[54]. Raw RNA sequencing data have been deposited in GenBank under BioProject ID PRJNA962685. The STRING version 11 resource[45] is available at https://string-db.org/. Publicly available insect genome assemblies and RNA sequencing data are from National Center for Biotechnology Information (NCBI) Genome browser (https://www.ncbi.nlm.nih.gov/datasets/genome/) and the NCBI Sequence Read Archive browser (https://www.ncbi.nlm.nih.gov/sra/)[55]. The OrthoDB version 10.1 resource[56] is available at https://v10-1.orthodb.org/. The lifespans of 43 insects are available at the Animal Diversity Web (https://animaldiversity.org/)[57]. All other data supporting the findings of this study are available as source data or from the corresponding authors upon reasonable request. Source data are provided with this paper.

References

1. Cooper, G. M. *The Cell: A Molecular Approach* (Sinauer Associates, 2000).
2. Sloan, D. B. et al. Cytonuclear integration and co-evolution. *Nat. Rev. Genet.* **19**, 635–648 (2018).
3. López-Otín, C., Blasco, M. A., Partridge, L., Serrano, M. & Kroemer, G. Hallmarks of aging: an expanding universe. *Cell* **186**, 243–278 (2023).
4. Bao, H. et al. Biomarkers of aging. *Sci. China Life Sci.* **66**, 893–1066 (2023).
5. Nunnari, J. & Suomalainen, A. Mitochondria: in sickness and in health. *Cell* **148**, 1145–1159 (2012).
6. McInnes, J. Mitochondrial-associated metabolic disorders: foundations, pathologies and recent progress. *Nutr. Metab. (Lond.)* **10**, 63 (2013).
7. Weaver, R. J., Rabinowitz, S., Thueson, K. & Havird, J. C. Genomic signatures of mitonuclear coevolution in mammals. *Mol. Biol. Evol.* **39**, msac233 (2022).

8. Piccinini, G. et al. Mitonuclear coevolution, but not nuclear compensation, drives evolution of OXPHOS complexes in bivalves. *Mol. Biol. Evol.* **38**, 2597–2614 (2021).
9. Yan, Z., Ye, G. & Werren, J. H. Evolutionary rate correlation between mitochondrial-encoded and mitochondria-associated nuclear-encoded proteins in insects. *Mol. Biol. Evol.* **36**, 1022–1036 (2019).
10. Woodson, J. D. & Chory, J. Coordination of gene expression between organellar and nuclear genomes. *Nat. Rev. Genet.* **9**, 383–395 (2008).
11. Cohen, H. Y. et al. Calorie restriction promotes mammalian cell survival by inducing the SIRT1 deacetylase. *Science* **305**, 390–392 (2004).
12. Stork, N. E. How many species of insects and other terrestrial arthropods are there on Earth? *Annu. Rev. Entomol.* **63**, 31–45 (2018).
13. Misof, B. et al. Phylogenomics resolves the timing and pattern of insect evolution. *Science* **346**, 763–767 (2014).
14. Zhou, J. et al. Large-scale RNAi screen identified Dhpr as a regulator of mitochondrial morphology and tissue homeostasis. *Sci. Adv.* **5**, eaax0365 (2019).
15. Jumper, J. et al. Highly accurate protein structure prediction with AlphaFold. *Nature* **596**, 583–589 (2021).
16. Ashbrook, D. G. et al. A platform for experimental precision medicine: the extended BXD mouse family. *Cell Syst.* **12**, 235–247. e9 (2021).
17. Bajgiran, M., Azlan, A., Shamsuddin, S., Azzam, G. & Halim, M. A. Data on RNA-seq analysis of *Drosophila melanogaster* during ageing. *Data Br.* **38**, 107413 (2021).
18. Fu, S., Zhang, J. & Xu, H. A genome-wide identification and analysis of the homeobox genes in the brown planthopper, *Nilaparvata lugens* (Hemiptera: Delphacidae). *Arch. Insect Biochem. Physiol.* **108**, e21833 (2021).
19. Du, Y. et al. Contact chemosensory genes identified in leg transcriptome of *Apis cerana cerana* (Hymenoptera: Apidae). *J. Econ. Entomol.* **112**, 2015–2029 (2019).
20. Xiong, G.-H. et al. High throughput profiling of the cotton bollworm *Helicoverpa armigera* immunotranscriptome during the fungal and bacterial infections. *BMC Genomics* **16**, 321 (2015).
21. Ferrarini, M. G. et al. Coordination of host and endosymbiont gene expression governs endosymbiont growth and elimination in the cereal weevil *Sitophilus* spp. *Microbiome* **11**, 274 (2023).
22. Steenwyk, J. L. et al. An orthologous gene coevolution network provides insight into eukaryotic cellular and genomic structure and function. *Sci. Adv.* **8**, eabn0105 (2022).
23. Clark, N. L., Alani, E. & Aquadro, C. F. Evolutionary rate covariation reveals shared functionality and coexpression of genes. *Genome Res.* **22**, 714–720 (2012).
24. Hall, B. S., Barnett, Y. A., Crofts, J. J. & Chuzhanova, N. Identification of novel genes associated with longevity in *Drosophila melanogaster*—a computational approach. *Aging (Albany NY)* **11**, 11244–11267 (2019).
25. Lu, T.-C. et al. Aging Fly Cell Atlas identifies exhaustive aging features at cellular resolution. *Science* **380**, eadg0934 (2023).
26. McCartney, D. L. et al. Genome-wide association studies identify 137 genetic loci for DNA methylation biomarkers of aging. *Genome Biol.* **22**, 194 (2021).
27. Burnett, C. et al. Absence of effects of Sir2 overexpression on lifespan in *C. elegans* and *Drosophila*. *Nature* **477**, 482–485 (2011).
28. Rogina, B. & Helfand, S. L. Sir2 mediates longevity in the fly through a pathway related to calorie restriction. *Proc. Natl Acad. Sci. USA* **101**, 15998–16003 (2004).
29. Hashimoto, T., Horikawa, M., Nomura, T. & Sakamoto, K. Nicotinamide adenine dinucleotide extends the lifespan of *Caenorhabditis elegans* mediated by *sir-2.1* and *daf-16*. *Biogerontology* **11**, 31–43 (2010).
30. Shen, H., Stoute, J. & Liu, K. F. Structural and catalytic roles of the human 18S rRNA methyltransferases DIMT1 in ribosome assembly and translation. *J. Biol. Chem.* **295**, 12058–12070 (2020).
31. Shen, H., Gonskikh, Y., Stoute, J. & Liu, K. F. Human DIMT1 generates $N_2^{6,6}$A-dimethylation–containing small RNAs. *J. Biol. Chem.* **297**, 101146 (2021).
32. Verma, G. et al. Ribosomal biogenesis regulator DIMT1 controls β-cell protein synthesis, mitochondrial function, and insulin secretion. *J. Biol. Chem.* **298**, 101692 (2022).
33. Liberman, N. et al. 18S rRNA methyltransferases DIMT1 and BUD23 drive intergenerational hormesis. *Mol. Cell* **83**, 3268–3282.e7 (2023).
34. Everman, E. R., Macdonald, S. J. & Kelly, J. K. The genetic basis of adaptation to copper pollution in *Drosophila melanogaster*. *Front. Genet.* **14**, 1144221 (2023).
35. Borchard, S. et al. The exceptional sensitivity of brain mitochondria to copper. *Toxicol. In Vitro* **51**, 11–22 (2018).
36. Di Cara, F., Duca, E., Dunbar, D. R., Cagney, G. & Heck, M. M. S. Invadolysin, a conserved lipid-droplet-associated metalloproteinase, is required for mitochondrial function in *Drosophila*. *J. Cell Sci.* **126**, 4769–4781 (2013).
37. Manni, M., Berkeley, M. R., Seppey, M., Simão, F. A. & Zdobnov, E. M. BUSCO update: novel and streamlined workflows along with broader and deeper phylogenetic coverage for scoring of eukaryotic, prokaryotic, and viral genomes. *Mol. Biol. Evol.* **38**, 4647–4654 (2021).
38. Levy Karin, E., Mirdita, M. & Söding, J. MetaEuk—sensitive, high-throughput gene discovery, and annotation for large-scale eukaryotic metagenomics. *Microbiome* **8**, 48 (2020).
39. Jin, J.-J. et al. GetOrganelle: a fast and versatile toolkit for accurate de novo assembly of organelle genomes. *Genome Biol.* **21**, 241 (2020).
40. Meng, G., Li, Y., Yang, C. & Liu, S. MitoZ: a toolkit for animal mitochondrial genome assembly, annotation and visualization. *Nucleic Acids Res.* **47**, e63 (2019).
41. Katoh, K. & Standley, D. M. MAFFT multiple sequence alignment software version 7: improvements in performance and usability. *Mol. Biol. Evol.* **30**, 772–780 (2013).
42. Capella-Gutierrez, S., Silla-Martinez, J. M. & Gabaldon, T. trimAl: a tool for automated alignment trimming in large-scale phylogenetic analyses. *Bioinformatics* **25**, 1972–1973 (2009).
43. Nguyen, L.-T., Schmidt, H. A., von Haeseler, A. & Minh, B. Q. IQ-TREE: a fast and effective stochastic algorithm for estimating maximum-likelihood phylogenies. *Mol. Biol. Evol.* **32**, 268–274 (2015).
44. Cameron, S. L. Insect mitochondrial genomics: implications for evolution and phylogeny. *Annu. Rev. Entomol.* **59**, 95–117 (2014).
45. Szklarczyk, D. et al. The STRING database in 2021: customizable protein–protein networks, and functional characterization of user-uploaded gene/measurement sets. *Nucleic Acids Res.* **49**, D605–D612 (2021).
46. Otasek, D., Morris, J. H., Bouças, J., Pico, A. R. & Demchak, B. Cytoscape Automation: empowering workflow-based network analysis. *Genome Biol.* **20**, 185 (2019).
47. Zhou, Y. et al. Metascape provides a biologist-oriented resource for the analysis of systems-level datasets. *Nat. Commun.* **10**, 1523 (2019).
48. Supek, F., Bošnjak, M., Škunca, N. & Šmuc, T. REVIGO summarizes and visualizes long lists of gene ontology terms. *PLoS ONE* **6**, e21800 (2011).
49. Bolger, A. M., Lohse, M. & Usadel, B. Trimmomatic: a flexible trimmer for Illumina sequence data. *Bioinformatics* **30**, 2114–2120 (2014).
50. Dobin, A. et al. STAR: ultrafast universal RNA-seq aligner. *Bioinformatics* **29**, 15–21 (2013).

51. Liao, Y., Smyth, G. K. & Shi, W. featureCounts: an efficient general purpose program for assigning sequence reads to genomic features. *Bioinformatics* **30**, 923–930 (2014).
52. Love, M. I., Huber, W. & Anders, S. Moderated estimation of fold change and dispersion for RNA-seq data with DESeq2. *Genome Biol.* **15**, 550 (2014).
53. Ge, S. X., Jung, D. & Yao, R. ShinyGO: a graphical gene-set enrichment tool for animals and plants. *Bioinformatics* **36**, 2628–2629 (2020).
54. Shen, X.-X. Identification of a longevity gene through evolutionary rate covariation of insect mito-nuclear genomes. *figshare* https://doi.org/10.6084/m9.figshare.22637761 (2024).
55. Benson, D. A. et al. GenBank. *Nucleic Acids Res.* **41**, D36–D42 (2012).
56. Zdobnov, E. M. et al. OrthoDB v9.1: cataloging evolutionary and functional annotations for animal, fungal, plant, archaeal, bacterial and viral orthologs. *Nucleic Acids Res.* **45**, D744–D749 (2017).
57. Yahnke, C. J., Dewey, T. & Myers, P. Animal diversity web as a teaching & learning tool to improve research & writing skills in college biology courses. *Am. Biol. Teach.* **75**, 494–498 (2013).
58. Keesey, T. M. *PhyloPic*; https://www.phylopic.org/

Acknowledgements

We thank X. Yin and J. Yang for constructive feedbacks. We also thank C. Tong and S. Liu for quantifying mitochondrial morphology. This work was conducted, in part, using the resources of the Information Technology Center and the State Key Laboratory of Computer-Aided Design & Computer Graphics at Zhejiang University. This work was supported by the National Key R&D Program of China (2022YFD1401600 to X.-X.S.); the National Science Foundation for Distinguished Young Scholars of Zhejiang Province (LR23C140001 to X.-X.S.); the National Natural Science Foundation of China (32071665 to X.-X.S., 32325044 to J.H., 32230015 and 32021001 to S.W. and 31922074 to Y.C.); the Fundamental Research Funds for the Central Universities (226-2023-00021 to X.-X.S. and 2021FZZX001-31 to Y.C.); the Zhejiang Provincial Natural Science Foundation of China (LZ23C140003 to J.H., LZ23C110002 to Y.Z., LZ23C020002 to R.P. and LR21C120002 to S.X.); the General Program of the National Natural Science Foundation of China (32371236 to Y.Z.); the New Cornerstone Science Foundation (S.W.); the Key International Joint Research Program of the National Natural Science Foundation of China (31920103005 to X.-x.C.); the National Science Foundation (DEB-2110404 to A.R.); and the National Institutes of Health/ National Institute of Allergy and Infectious Diseases (R01 AI153356 to A.R.).

Author contributions

X.-X.S. conceived and designed the study. X.-X.S., M.T., J.C., C.C., Z.S., J.X., J.Y., J.Z., G.-Z.O., C.L. and Y.X. performed computational analyses and experiments. X.-X.S., J.H., A.R., S.W., M.T., J.C., Y.C., Z.-R.Z., R.P., S.X., X.-x.C. and Y.Z. interpreted results. X.-X.S. wrote the paper, with input from all authors. X.-X.S., M.T., J.H., A.R., S.W. and Y.Z. edited the paper.

Competing interests

A.R. is a scientific consultant for LifeMine Therapeutics, Inc. The other authors declare no competing interests.

Additional information

Extended data is available for this paper at https://doi.org/10.1038/s43587-024-00641-z.

Supplementary information The online version contains supplementary material available at https://doi.org/10.1038/s43587-024-00641-z.

Correspondence and requests for materials should be addressed to Sibao Wang, Jianhua Huang or Xing-Xing Shen.

Peer review information *Nature Aging* thanks Mark Harrison, David Rand, Li Zhao and the other, anonymous, reviewer(s) for their contribution to the peer review of this work.

https://doi.org/10.1038/s43587-024-00641-z

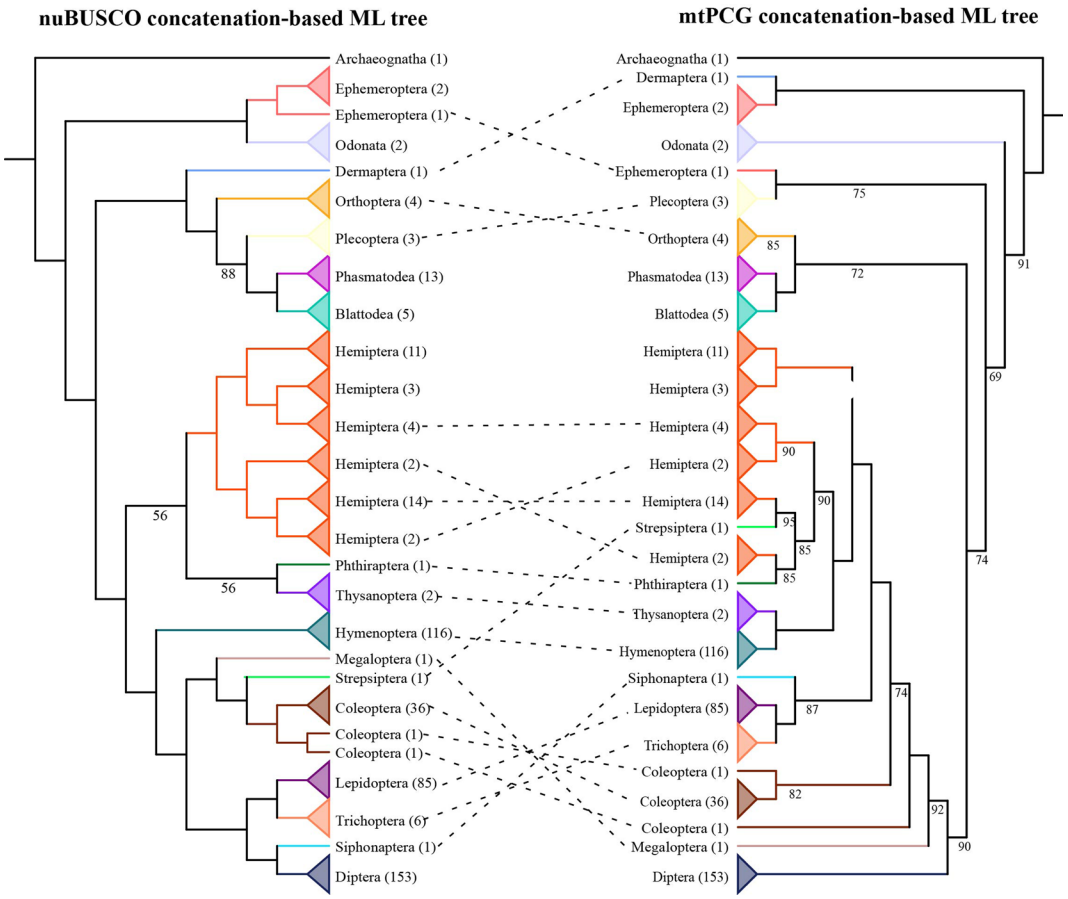

Extended Data Fig. 1 | Comparison of the higher-level phylogenies inferred from the analyses of 1,417 nuclear BUSCO amino acid genes (left panel) and 13 mitochondrial amino acid genes (right panel). Branch support values near internodes / internal branches correspond to ultrafast bootstrap support. Only support values smaller than 95% are shown. The number in parenthesis is the number of species for each collapsed clade. The conflicting relationships between nuBUCSO phylogeny and mtPCG phylogeny indicate dashed lines. Two complete phylogenies are given in Supplementary Figs. 3 and 4.

https://doi.org/10.1038/s43587-024-00641-z

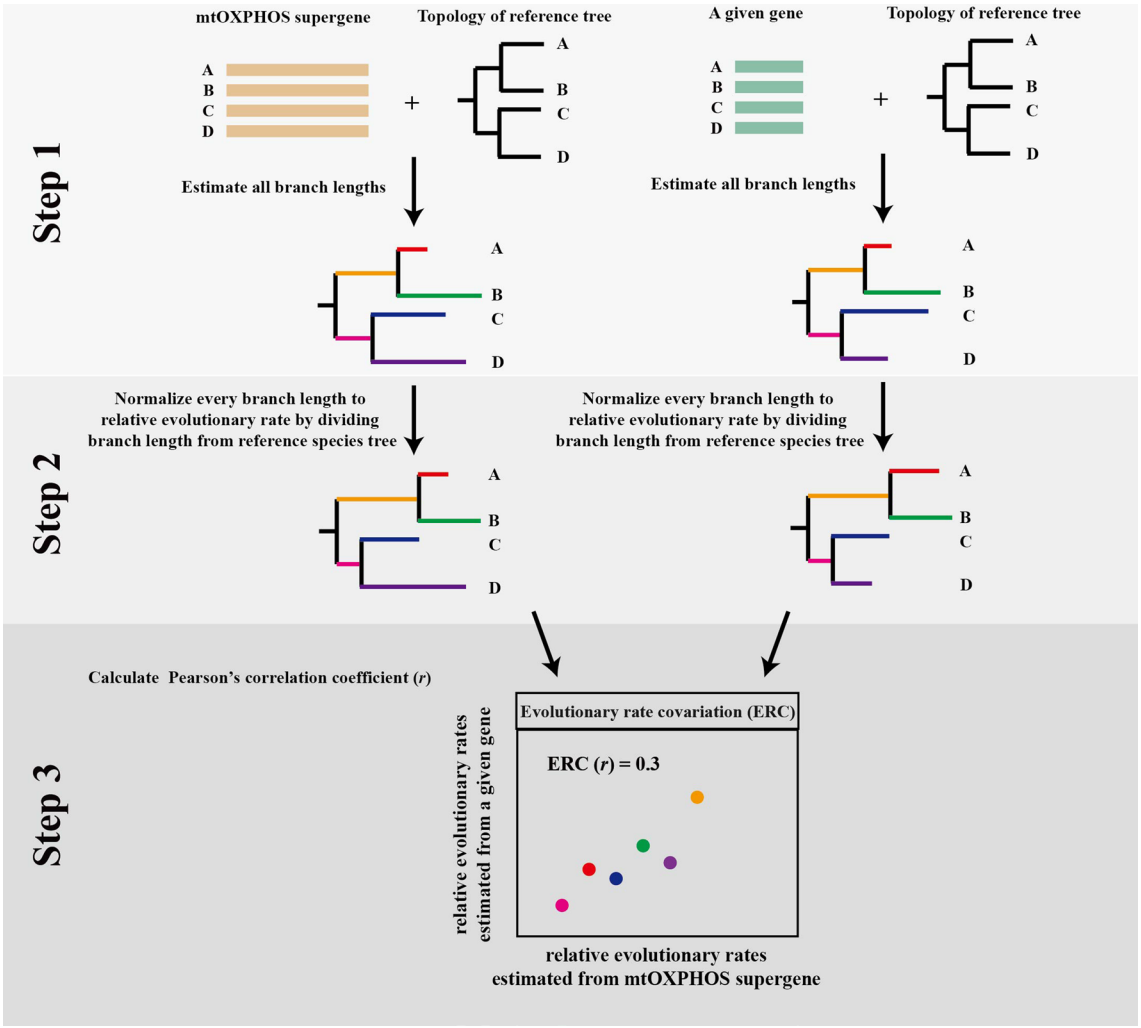

Extended Data Fig. 2 | The schematic workflow used for the calculation of the evolutionary rate covariation (ERC). Evolutionary rate covariation (ERC) was the Pearson's correlation coefficient (*r*) between relative evolutionary rates estimated from each branch of the phylogeny inferred from a given gene and those estimated from each branch of the phylogeny inferred from the mtOXPHOS supergene (concatenated 13 mtOXPHOS genes). The reference (or background) species tree is from the Fig. 1a. A detailed description of the analyses performed in each step of the workflow is provided in the Methods.

https://doi.org/10.1038/s43587-024-00641-z

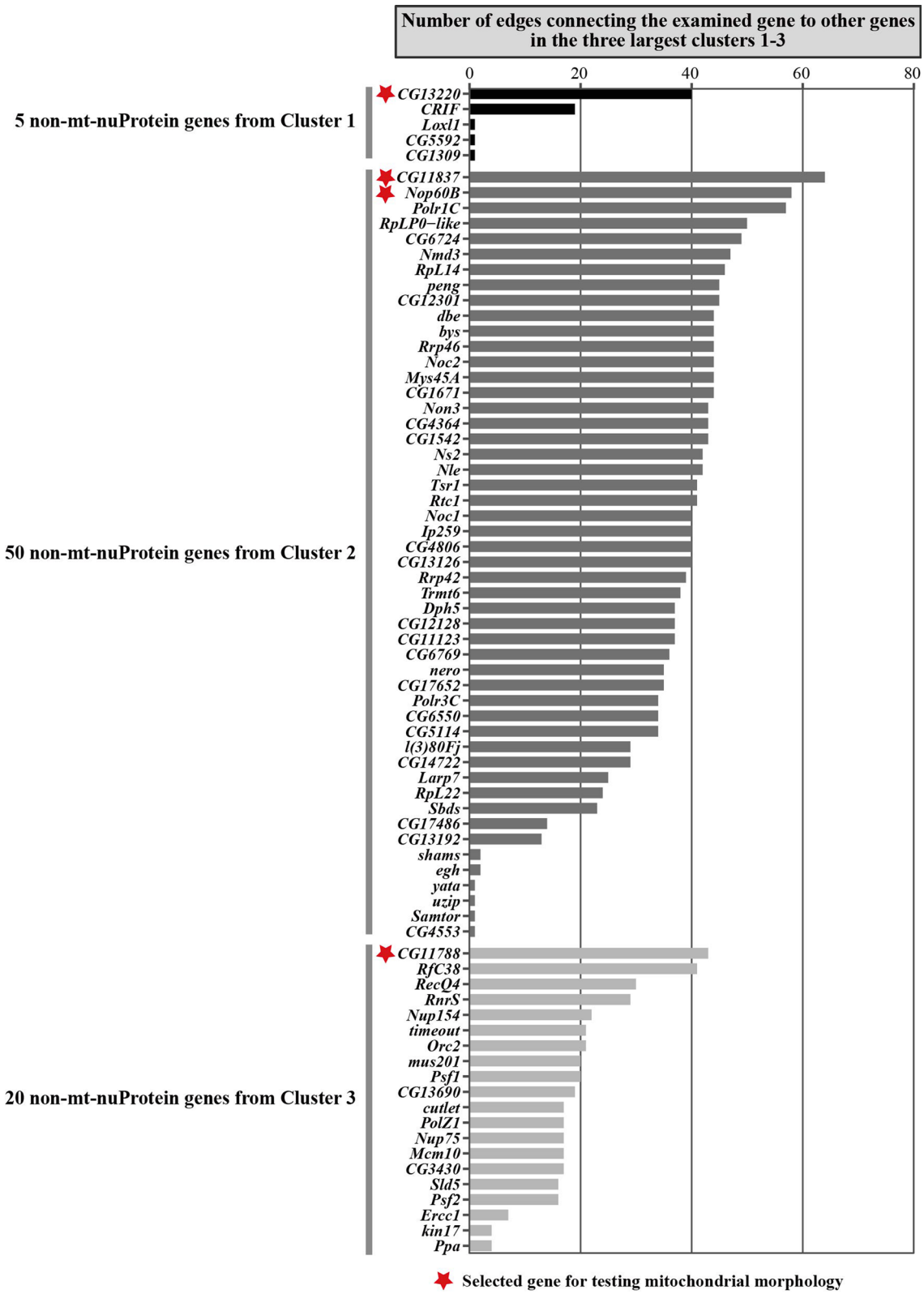

Extended Data Fig. 3 | The histogram of connectivity for each of the 75 non-mt-nuProtein genes in three largest Clusters 1-3. After identifying 75 non-mt-nuProtein genes based on the protein-protein association network (Fig. 3b), we further examined the connectivity (that is, the number of edges connecting the examined gene to other genes) for each of the 75 non-mt-nuProtein genes within three largest Clusters 1-3. Four genes with red stars, namely, *CG13220*, *CG11837*, and *CG11788*, which displayed the highest connectivity levels in their respective clusters, as well as *Nop60B*, which ranked as the second-highest in connectivity within the largest Cluster 2 that contains 50 genes (~ 67%) out of the 75 non-mt-nuProtein genes, were used to investigate their impact on mitochondrial morphology.

https://doi.org/10.1038/s43587-024-00641-z

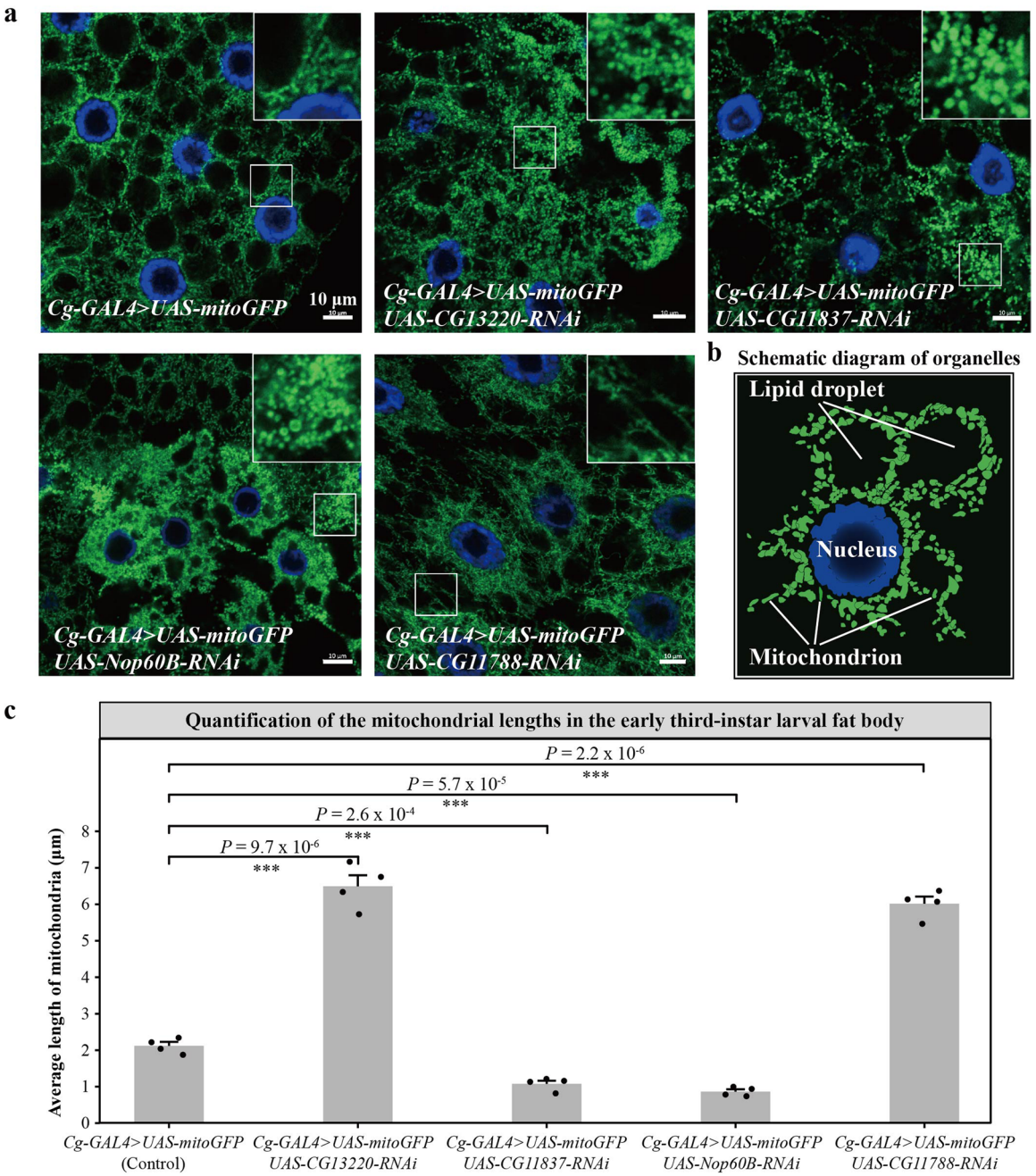

Extended Data Fig. 4 | Effect of RNA interference of four non-mitochondria-targeted nuclear candidate genes on mitochondrial morphology. We chose *CG13220, CG11837, CG11788*, and *Nop60B* to examine their effect on fruit fly mitochondrial morphologies. The *Cg-GAL4 > UAS-mitoGFP* line was crossed with the four *UAS-RNAi* lines (*UAS-CG13220-RNAi, UAS-CG11837-RNAi, UAS-CG11788-RNAi*, and *UAS-Nop60B-RNAi*), respectively. The early third-instar larval fat body was used for investigating mitochondrial morphology for each genotype. **a**, For each image, the boxes in the top right corners of the individual panels are magnifications that show mitochondrial morphology in greater detail. The genotypes are specified in the bottom left corners of the individual panels. We included three additional representative images for each genotype in Supplementary Fig. 10a, in addition to the one already provided. Scale bars = 10 μm. **b**, Illustration of the simplified organelle components, determined and stained from the control (*Cg-GAL4 > UAS-mitoGFP*) early third-instar larval fat body. **c**, For a given genotype's confocal image, we measured and averaged the length of mitochondria from each of five randomly selected areas (25μm x 25μm) in the early third-instar larval fat body. n = 4 biologically independent experiments for each genotype. Data represent mean ± SD. *P* values were calculated using a two-tailed t test. ***$P \leq 0.001$.

https://doi.org/10.1038/s43587-024-00641-z

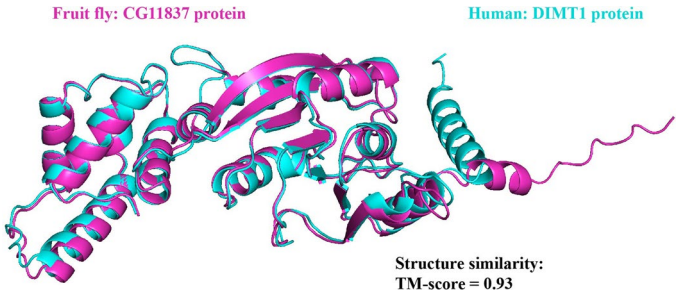

Extended Data Fig. 5 | A superposition between two protein structures. Protein structures of fruit fly CG11837 and human DIMT1 were retrieved from the Alphafold2 database (https://alphafold.ebi.ac.uk/), respectively. TM-score in structure similarity is 0.93.

https://doi.org/10.1038/s43587-024-00641-z

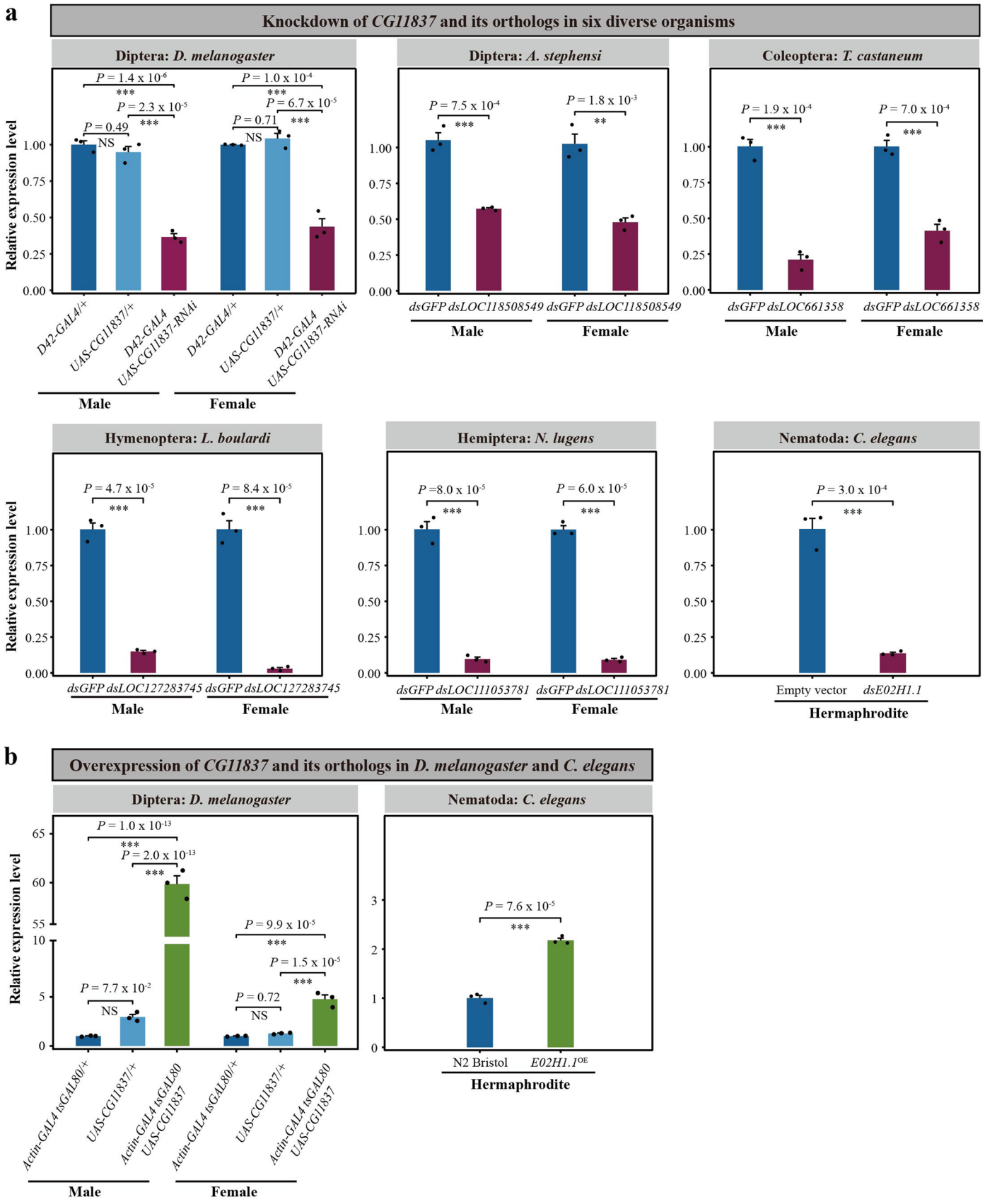

Extended Data Fig. 6 | See next page for caption.

https://doi.org/10.1038/s43587-024-00641-z

Extended Data Fig. 6 | The efficiencies of knockdown and overexpression of *CG11837*. **a**, The efficiencies of knockdown of *CG11837* and its orthologs on both sexes. Note that the worm was not assessed for two sexes, as worms are hermaphrodites. Fruit fly used *D42-GAL4/+* and *UAS-CG11837-RNAi/+* as two genetic controls; mosquito, beetle, bee, and brown planthopper used *dsGFP* as controls; worm used empty vector as a control. n = 3 biologically independent experiments for each genotype. Data represent mean ± SD. *P* values were calculated using a two-tailed t test. NS $P > 0.05$; $^{*}P \leq 0.05$; $^{**}P \leq 0.01$; $^{***}P \leq 0.001$. **b**, The efficiency of overexpression of *CG11837* in fruit fly and *E02H1.1* (an ortholog of *CG11837)* in worm. Fruit fly used *Actin-GAL4 tsGAL80/+* and *UAS-CG11837/+* as two genetic controls; worm used the N2 Bristol strain as a control. Note that the worm was not assessed for two sexes, as worms are hermaphrodites. n = 3 biologically independent experiments for each genotype. Data represent mean ± SD. *P* values were calculated using a two-tailed t test. NS $P > 0.05$; $^{*}P \leq 0.05$; $^{**}P \leq 0.01$; $^{***}P \leq 0.001$. All examined organisms are 3-day-old adults.

https://doi.org/10.1038/s43587-024-00641-z

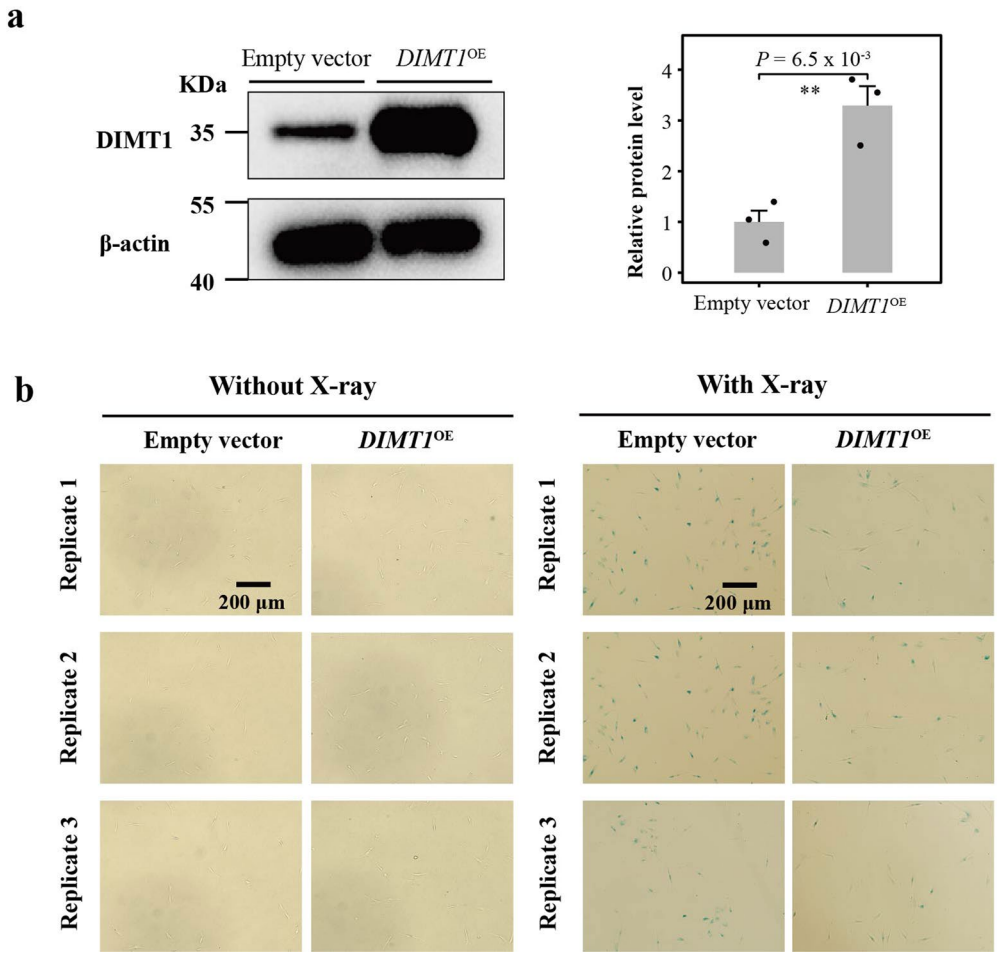

Extended Data Fig. 7 | Overexpression of *DIMT1* protects human cells in response to DNA damage. a, Western blot verifying the overexpression of *DIMT1* in human skin fibroblasts. n = 3 biologically independent experiments. Data represent mean ± SD. *P* value was calculated using a two-tailed t test. $^{**}P \leq 0.01$ and > 0.001. **b**, Senescence-associated β-galactosidase (SA-β-gal.) activity assay without (left panel) and with (right panel) X-ray. Cells were irradiated without or with 5 Gy X-ray. Ten days after irradiation, cells were re-seeded to 6-well plates and the next day, cells were stained for SA-β-gal. n = 3 biologically independent experiments. Scale bars = 200 μm.

https://doi.org/10.1038/s43587-024-00641-z

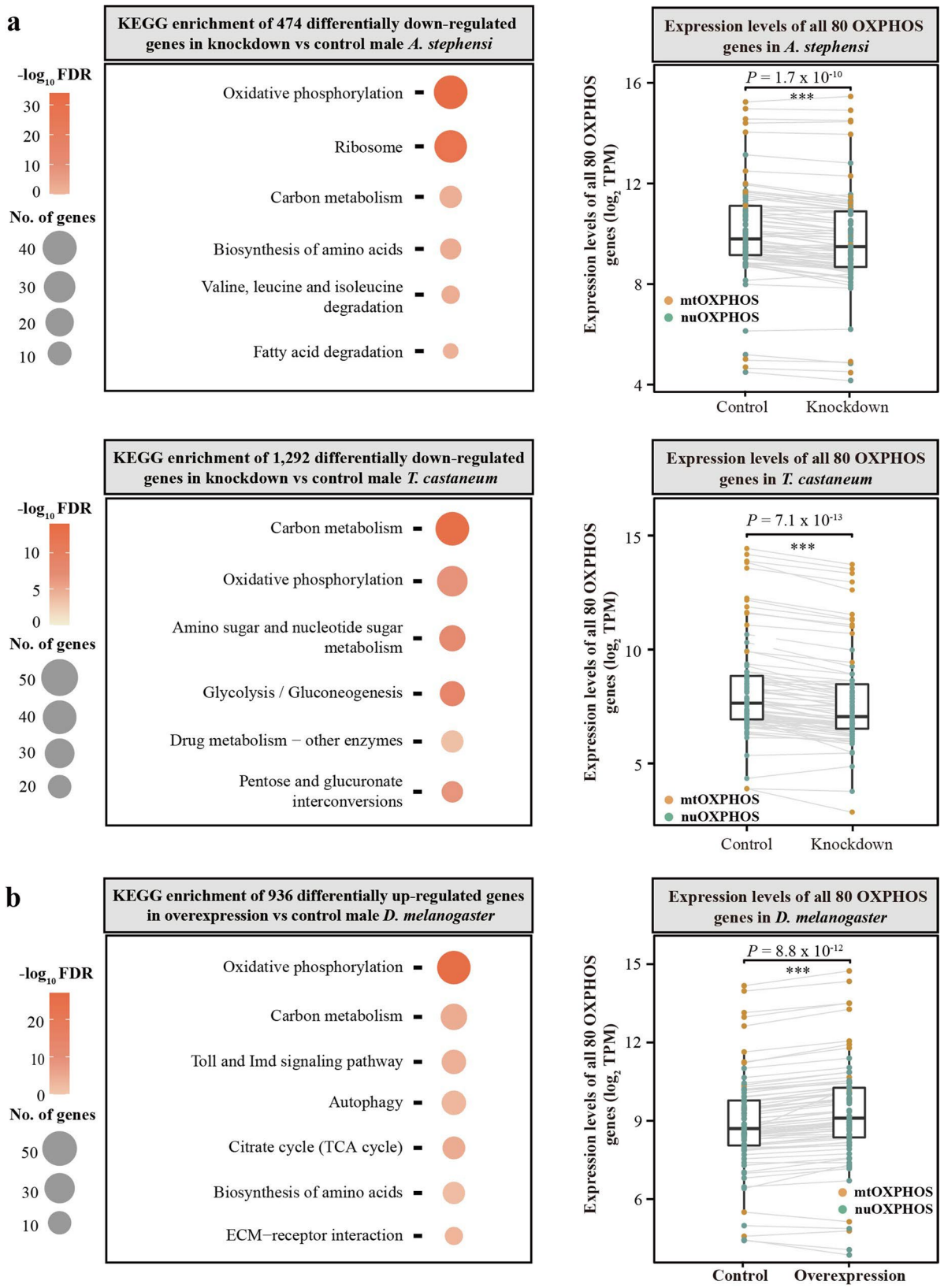

Extended Data Fig. 8 | Transcriptome data analysis for KEGG pathway enrichment and expression level of all 80 OXPHOS genes. a, KEGG pathway enrichment (left panel) and expression level of all OXPHOS genes (right panel) between *CG11837* knockdown and control male adults of 3-day-old mosquitos and 13-day-old beetles. A two paired Wilcoxon test was used to test whether the two sets of values (sample size = 80) are significantly different. ***$P \leq 0.001$. **b**, KEGG pathway enrichment (left panel) and expression level of all OXPHOS genes (right panel) between *CG11837* overexpression and control male adults of 3-day-old fruit files. A two paired Wilcoxon test was used to test whether the two sets of values (sample size = 80) are significantly different. ***$P \leq 0.001$.

https://doi.org/10.1038/s43587-024-00641-z

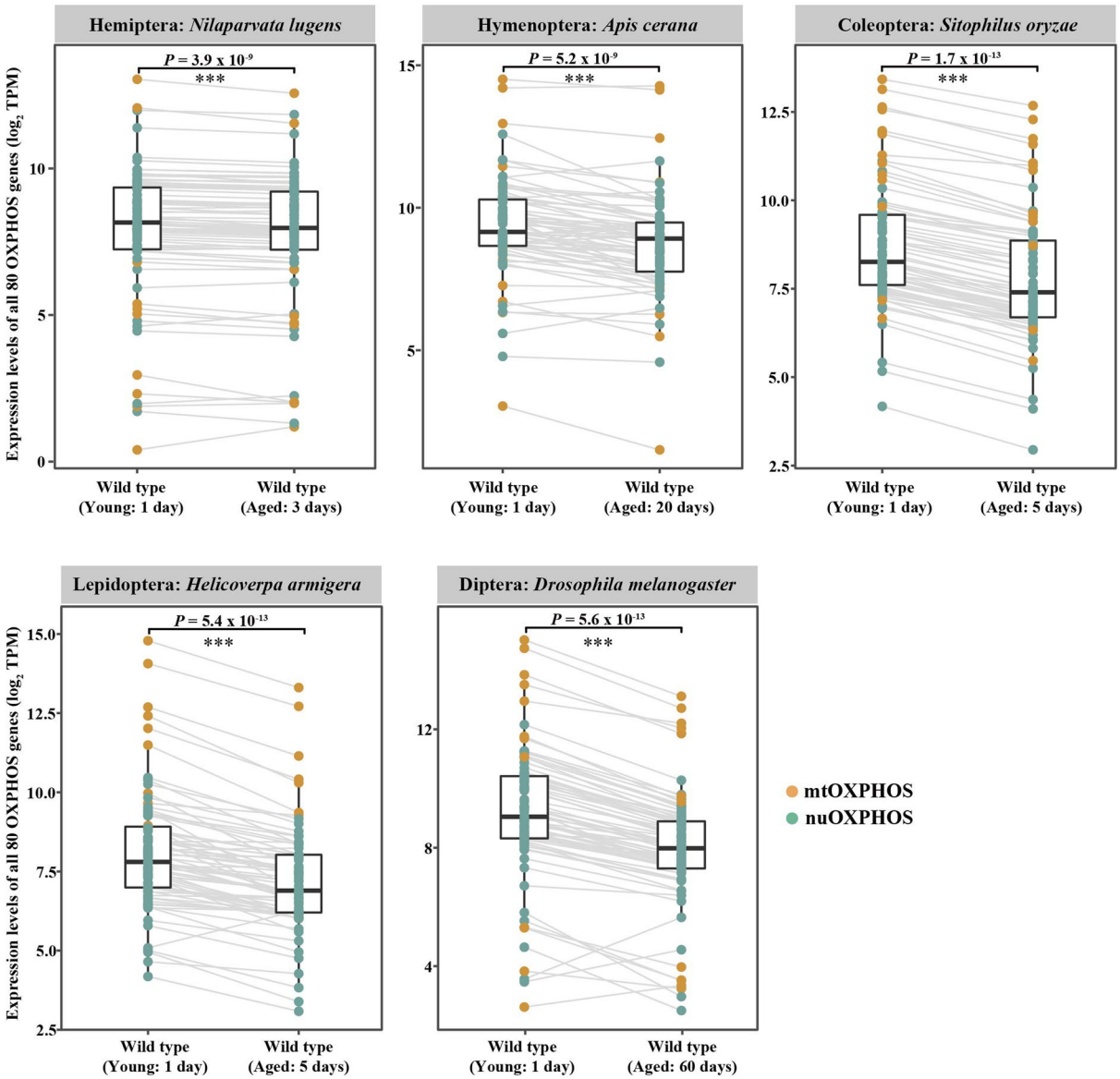

Extended Data Fig. 9 | Comparison of expression levels of the all 80 OXPHOS genes between young and aged adult insects. Note that expression levels of all OXPHOS genes for young and aged insects were calculated based on publicly available wild type adult whole body transcriptome data. *Nilaparvata lugens*: female; *Apis cerana*: female; *Sitophilus oryzae*: unknown sex; *Helicoverpa armigera*: unknown sex; *Drosophila melanogaster*: female + male. For each boxplot, the bottom, center and top represent 25th, 50th and 75th percentiles, respectively. Whiskers represent 1.5× interquartile range. Sample size = 80. Two-tailed paired Wilcoxon test was used to test whether the two sets of values are significantly different. ***$P \leq 0.001$.

nature portfolio

Corresponding author(s): Sibao Wang, Jianhua Huang, and Xing-Xing Shen

Last updated by author(s): Apr 21, 2024

Reporting Summary

Nature Portfolio wishes to improve the reproducibility of the work that we publish. This form provides structure for consistency and transparency in reporting. For further information on Nature Portfolio policies, see our Editorial Policies and the Editorial Policy Checklist.

Statistics

For all statistical analyses, confirm that the following items are present in the figure legend, table legend, main text, or Methods section.

n/a	Confirmed
☐	☒ The exact sample size (*n*) for each experimental group/condition, given as a discrete number and unit of measurement
☐	☒ A statement on whether measurements were taken from distinct samples or whether the same sample was measured repeatedly
☐	☒ The statistical test(s) used AND whether they are one- or two-sided *Only common tests should be described solely by name; describe more complex techniques in the Methods section.*
☐	☒ A description of all covariates tested
☐	☒ A description of any assumptions or corrections, such as tests of normality and adjustment for multiple comparisons
☐	☒ A full description of the statistical parameters including central tendency (e.g. means) or other basic estimates (e.g. regression coefficient) AND variation (e.g. standard deviation) or associated estimates of uncertainty (e.g. confidence intervals)
☐	☒ For null hypothesis testing, the test statistic (e.g. *F*, *t*, *r*) with confidence intervals, effect sizes, degrees of freedom and *P* value noted *Give P values as exact values whenever suitable.*
☒	☐ For Bayesian analysis, information on the choice of priors and Markov chain Monte Carlo settings
☒	☐ For hierarchical and complex designs, identification of the appropriate level for tests and full reporting of outcomes
☐	☒ Estimates of effect sizes (e.g. Cohen's *d*, Pearson's *r*), indicating how they were calculated

Our web collection on statistics for biologists contains articles on many of the points above.

Software and code

Policy information about availability of computer code

Data collection	No software or code was used for data collection.
Data analysis	BUSCO v 5.2.2 and MetaEuk v 5-34c21f2 were used for assessing assembly completeness. GetOrganelle v1.7.3.5 and MitoZ v2.3 were used for annotating the mitochondrial genomes. MAFFT v7.299b, trimAl v1.4.rev15, and IQ-TREE v1.6.8 were used for constructing phylogenetic matrix and inferring phylogenetic trees. Cytoscape v3.9.0, Metascape v3.5, and REVIGO v20150217beta were used for identifying of mitochondria-associated nuclear genes. Trimmomatic v0.39, STAR v2.7.10a, featureCounts v2.0.1, DESeq2 v1.30.152, and ShinyGO 0.77 53 were used for analyzing transcriptome data. All statistical analyses were performed in R v. 3.4.2.

For manuscripts utilizing custom algorithms or software that are central to the research but not yet described in published literature, software must be made available to editors and reviewers. We strongly encourage code deposition in a community repository (e.g. GitHub). See the Nature Portfolio guidelines for submitting code & software for further information.

Data

Policy information about availability of data

All manuscripts must include a data availability statement. This statement should provide the following information, where applicable:

- Accession codes, unique identifiers, or web links for publicly available datasets
- A description of any restrictions on data availability
- For clinical datasets or third party data, please ensure that the statement adheres to our policy

All mitochondrial genomes, phylogenomic matrix, gene trees, and summary statistics as well as 3D protein structures of 75 non-mitochondria-targeted nuclear proteins, are available on the figshare repository (https://doi.org/10.6084/m9.figshare.22637761). Raw RNA sequencing data has been deposited in GenBank under Bioproject ID: PRJNA962685. The STRING v11 resource is available at https://string-db.org/. Publicly available insect genome assemblies and RNA-seq data are from NCBI's Genome Browser (https://www.ncbi.nlm.nih.gov/datasets/genome/) and NCBI's Sequence Read Archive (SRA) Browser (https://www.ncbi.nlm.nih.gov/sra/). OrthoDB Version 10.1 resource is available at https://v10-1.orthodb.org/. The lifespans of 43 insects are available at Animal Diversity Web (ADW) (https://animaldiversity.org/). All other data supporting the findings of this study are available as source data or from the corresponding author upon request.

Research involving human participants, their data, or biological material

Policy information about studies with human participants or human data. See also policy information about sex, gender (identity/presentation), and sexual orientation and race, ethnicity and racism.

Reporting on sex and gender	not applicable
Reporting on race, ethnicity, or other socially relevant groupings	not applicable
Population characteristics	not applicable
Recruitment	not applicable
Ethics oversight	not applicable

Note that full information on the approval of the study protocol must also be provided in the manuscript.

Field-specific reporting

Please select the one below that is the best fit for your research. If you are not sure, read the appropriate sections before making your selection.

☒ Life sciences ☐ Behavioural & social sciences ☐ Ecological, evolutionary & environmental sciences

For a reference copy of the document with all sections, see nature.com/documents/nr-reporting-summary-flat.pdf

Life sciences study design

All studies must disclose on these points even when the disclosure is negative.

Sample size	We did not use a statistical method to predetermine the sample size; instead, sample sizes were guided by practical considerations and the availability of insect mitochondrial and nuclear genomes in NCBI as of 9 May 2020.
Data exclusions	No data were excluded from the analyses.
Replication	Experiments were performed with three or more biological replicates.
Randomization	Randomization was not employed in our study design, as there was no intention to balance differences.
Blinding	Blinding was not incorporated into our experimental design as we utilized multiple biological and technical replicates. Therefore, none of the experiments conducted were blinded.

Behavioural & social sciences study design

All studies must disclose on these points even when the disclosure is negative.

Study description	*Briefly describe the study type including whether data are quantitative, qualitative, or mixed-methods (e.g. qualitative cross-sectional, quantitative experimental, mixed-methods case study).*

Research sample	*State the research sample (e.g. Harvard university undergraduates, villagers in rural India) and provide relevant demographic information (e.g. age, sex) and indicate whether the sample is representative. Provide a rationale for the study sample chosen. For studies involving existing datasets, please describe the dataset and source.*
Sampling strategy	*Describe the sampling procedure (e.g. random, snowball, stratified, convenience). Describe the statistical methods that were used to predetermine sample size OR if no sample-size calculation was performed, describe how sample sizes were chosen and provide a rationale for why these sample sizes are sufficient. For qualitative data, please indicate whether data saturation was considered, and what criteria were used to decide that no further sampling was needed.*
Data collection	*Provide details about the data collection procedure, including the instruments or devices used to record the data (e.g. pen and paper, computer, eye tracker, video or audio equipment) whether anyone was present besides the participant(s) and the researcher, and whether the researcher was blind to experimental condition and/or the study hypothesis during data collection.*
Timing	*Indicate the start and stop dates of data collection. If there is a gap between collection periods, state the dates for each sample cohort.*
Data exclusions	*If no data were excluded from the analyses, state so OR if data were excluded, provide the exact number of exclusions and the rationale behind them, indicating whether exclusion criteria were pre-established.*
Non-participation	*State how many participants dropped out/declined participation and the reason(s) given OR provide response rate OR state that no participants dropped out/declined participation.*
Randomization	*If participants were not allocated into experimental groups, state so OR describe how participants were allocated to groups, and if allocation was not random, describe how covariates were controlled.*

Ecological, evolutionary & environmental sciences study design

All studies must disclose on these points even when the disclosure is negative.

Study description	*Briefly describe the study. For quantitative data include treatment factors and interactions, design structure (e.g. factorial, nested, hierarchical), nature and number of experimental units and replicates.*
Research sample	*Describe the research sample (e.g. a group of tagged Passer domesticus, all Stenocereus thurberi within Organ Pipe Cactus National Monument), and provide a rationale for the sample choice. When relevant, describe the organism taxa, source, sex, age range and any manipulations. State what population the sample is meant to represent when applicable. For studies involving existing datasets, describe the data and its source.*
Sampling strategy	*Note the sampling procedure. Describe the statistical methods that were used to predetermine sample size OR if no sample-size calculation was performed, describe how sample sizes were chosen and provide a rationale for why these sample sizes are sufficient.*
Data collection	*Describe the data collection procedure, including who recorded the data and how.*
Timing and spatial scale	*Indicate the start and stop dates of data collection, noting the frequency and periodicity of sampling and providing a rationale for these choices. If there is a gap between collection periods, state the dates for each sample cohort. Specify the spatial scale from which the data are taken*
Data exclusions	*If no data were excluded from the analyses, state so OR if data were excluded, describe the exclusions and the rationale behind them, indicating whether exclusion criteria were pre-established.*
Reproducibility	*Describe the measures taken to verify the reproducibility of experimental findings. For each experiment, note whether any attempts to repeat the experiment failed OR state that all attempts to repeat the experiment were successful.*
Randomization	*Describe how samples/organisms/participants were allocated into groups. If allocation was not random, describe how covariates were controlled. If this is not relevant to your study, explain why.*
Blinding	*Describe the extent of blinding used during data acquisition and analysis. If blinding was not possible, describe why OR explain why blinding was not relevant to your study.*

Did the study involve field work? ☐ Yes ☐ No

Field work, collection and transport

Field conditions	*Describe the study conditions for field work, providing relevant parameters (e.g. temperature, rainfall).*
Location	*State the location of the sampling or experiment, providing relevant parameters (e.g. latitude and longitude, elevation, water depth).*
Access & import/export	*Describe the efforts you have made to access habitats and to collect and import/export your samples in a responsible manner and in*

Access & import/export	*compliance with local, national and international laws, noting any permits that were obtained (give the name of the issuing authority, the date of issue, and any identifying information).*
Disturbance	*Describe any disturbance caused by the study and how it was minimized.*

Reporting for specific materials, systems and methods

We require information from authors about some types of materials, experimental systems and methods used in many studies. Here, indicate whether each material, system or method listed is relevant to your study. If you are not sure if a list item applies to your research, read the appropriate section before selecting a response.

Materials & experimental systems

n/a	Involved in the study
☐	☒ Antibodies
☐	☒ Eukaryotic cell lines
☒	☐ Palaeontology and archaeology
☐	☒ Animals and other organisms
☒	☐ Clinical data
☒	☐ Dual use research of concern
☒	☐ Plants

Methods

n/a	Involved in the study
☒	☐ ChIP-seq
☒	☐ Flow cytometry
☒	☐ MRI-based neuroimaging

Antibodies

Antibodies used	DIMT1(abcam ab271003: 1:1000 for western blot), BrdU (Thermo Fisher 11-5071-42: 1:200 for immunofluorescence)
Validation	Immunoblot - DIMT1 – abcam, ab271003

Eukaryotic cell lines

Policy information about cell lines and Sex and Gender in Research

Cell line source(s)	Human primary skin fibroblasts HCA2 were obtained from Huffington Center on Aging and named by Olivia Pereira-Smith.
Authentication	Fibroblast cell lines were authenticated using Short Tandem Repeat (STR) analysis as described in 2012 in ANSI Standard (ASN-0002) by the ATCC Standards Development Organization (SDO) and in Capes-Davis et al., Match criteria for human cell line authentication: Where do we draw the line? Int J Caner, 2023, 132(11): 2510-9.
Mycoplasma contamination	All cells are mycoplasma-free with regular checks performed by a LookOut Mycoplasma PCR Detection Kit (MP0035, Sigma-Aldrich).
Commonly misidentified lines (See ICLAC register)	None of the cell lines used in this study are listed in the International Cell Line Authentication Committee (ICLAC) database.

Palaeontology and Archaeology

Specimen provenance	*Provide provenance information for specimens and describe permits that were obtained for the work (including the name of the issuing authority, the date of issue, and any identifying information). Permits should encompass collection and, where applicable, export.*
Specimen deposition	*Indicate where the specimens have been deposited to permit free access by other researchers.*
Dating methods	*If new dates are provided, describe how they were obtained (e.g. collection, storage, sample pretreatment and measurement), where they were obtained (i.e. lab name), the calibration program and the protocol for quality assurance OR state that no new dates are provided.*

☐ Tick this box to confirm that the raw and calibrated dates are available in the paper or in Supplementary Information.

Ethics oversight	*Identify the organization(s) that approved or provided guidance on the study protocol, OR state that no ethical approval or guidance was required and explain why not.*

Note that full information on the approval of the study protocol must also be provided in the manuscript.

Animals and other research organisms

Policy information about studies involving animals; ARRIVE guidelines recommended for reporting animal research, and Sex and Gender in Research

Laboratory animals	Details about all six examined species are provided in the Methods. 3-day-old adult Drosophila melanogaster (W1118)3-day-old adult Anopheles stephensi (Dutch strain)3-day-old adult Tribolium castaneum (Tcas_zju), 3-day-old adult Leptopilina boulardi (Lb14), 3-day-old adult Nilaparvata lugens (Stal), and 3-day-old adult Caenorhabditis elegans (N2).
Wild animals	No wild animals were used in the study.
Reporting on sex	The findings in this study apply to both male and female animals.
Field-collected samples	No field-collected samples were used.
Ethics oversight	Since all examined species were from the labs, there was no need for ethical approval.

Note that full information on the approval of the study protocol must also be provided in the manuscript.

Clinical data

Policy information about clinical studies

All manuscripts should comply with the ICMJE guidelines for publication of clinical research and a completed CONSORT checklist must be included with all submissions.

Clinical trial registration	*Provide the trial registration number from ClinicalTrials.gov or an equivalent agency.*
Study protocol	*Note where the full trial protocol can be accessed OR if not available, explain why.*
Data collection	*Describe the settings and locales of data collection, noting the time periods of recruitment and data collection.*
Outcomes	*Describe how you pre-defined primary and secondary outcome measures and how you assessed these measures.*

Dual use research of concern

Policy information about dual use research of concern

Hazards

Could the accidental, deliberate or reckless misuse of agents or technologies generated in the work, or the application of information presented in the manuscript, pose a threat to:

No	Yes	
☐	☐	Public health
☐	☐	National security
☐	☐	Crops and/or livestock
☐	☐	Ecosystems
☐	☐	Any other significant area

Experiments of concern

Does the work involve any of these experiments of concern:

No	Yes	
☐	☐	Demonstrate how to render a vaccine ineffective
☐	☐	Confer resistance to therapeutically useful antibiotics or antiviral agents
☐	☐	Enhance the virulence of a pathogen or render a nonpathogen virulent
☐	☐	Increase transmissibility of a pathogen
☐	☐	Alter the host range of a pathogen
☐	☐	Enable evasion of diagnostic/detection modalities
☐	☐	Enable the weaponization of a biological agent or toxin
☐	☐	Any other potentially harmful combination of experiments and agents

Plants

Seed stocks: not applicable

Novel plant genotypes: not applicable

Authentication: not applicable

ChIP-seq

Data deposition

☐ Confirm that both raw and final processed data have been deposited in a public database such as GEO.

☐ Confirm that you have deposited or provided access to graph files (e.g. BED files) for the called peaks.

Data access links
May remain private before publication.
For "Initial submission" or "Revised version" documents, provide reviewer access links. For your "Final submission" document, provide a link to the deposited data.

Files in database submission
Provide a list of all files available in the database submission.

Genome browser session
(e.g. UCSC)
Provide a link to an anonymized genome browser session for "Initial submission" and "Revised version" documents only, to enable peer review. Write "no longer applicable" for "Final submission" documents.

Methodology

Replicates
Describe the experimental replicates, specifying number, type and replicate agreement.

Sequencing depth
Describe the sequencing depth for each experiment, providing the total number of reads, uniquely mapped reads, length of reads and whether they were paired- or single-end.

Antibodies
Describe the antibodies used for the ChIP-seq experiments; as applicable, provide supplier name, catalog number, clone name, and lot number.

Peak calling parameters
Specify the command line program and parameters used for read mapping and peak calling, including the ChIP, control and index files used.

Data quality
Describe the methods used to ensure data quality in full detail, including how many peaks are at FDR 5% and above 5-fold enrichment.

Software
Describe the software used to collect and analyze the ChIP-seq data. For custom code that has been deposited into a community repository, provide accession details.

Flow Cytometry

Plots

Confirm that:

☐ The axis labels state the marker and fluorochrome used (e.g. CD4-FITC).

☐ The axis scales are clearly visible. Include numbers along axes only for bottom left plot of group (a 'group' is an analysis of identical markers).

☐ All plots are contour plots with outliers or pseudocolor plots.

☐ A numerical value for number of cells or percentage (with statistics) is provided.

Methodology

Sample preparation
Describe the sample preparation, detailing the biological source of the cells and any tissue processing steps used.

Instrument
Identify the instrument used for data collection, specifying make and model number.

Software
Describe the software used to collect and analyze the flow cytometry data. For custom code that has been deposited into a community repository, provide accession details.

Cell population abundance

Describe the abundance of the relevant cell populations within post-sort fractions, providing details on the purity of the samples and how it was determined.

Gating strategy

Describe the gating strategy used for all relevant experiments, specifying the preliminary FSC/SSC gates of the starting cell population, indicating where boundaries between "positive" and "negative" staining cell populations are defined.

☐ Tick this box to confirm that a figure exemplifying the gating strategy is provided in the Supplementary Information.

Magnetic resonance imaging

Experimental design

Design type

Indicate task or resting state; event-related or block design.

Design specifications

Specify the number of blocks, trials or experimental units per session and/or subject, and specify the length of each trial or block (if trials are blocked) and interval between trials.

Behavioral performance measures

State number and/or type of variables recorded (e.g. correct button press, response time) and what statistics were used to establish that the subjects were performing the task as expected (e.g. mean, range, and/or standard deviation across subjects).

Acquisition

Imaging type(s)

Specify: functional, structural, diffusion, perfusion.

Field strength

Specify in Tesla

Sequence & imaging parameters

Specify the pulse sequence type (gradient echo, spin echo, etc.), imaging type (EPI, spiral, etc.), field of view, matrix size, slice thickness, orientation and TE/TR/flip angle.

Area of acquisition

State whether a whole brain scan was used OR define the area of acquisition, describing how the region was determined.

Diffusion MRI ☐ Used ☐ Not used

Preprocessing

Preprocessing software

Provide detail on software version and revision number and on specific parameters (model/functions, brain extraction, segmentation, smoothing kernel size, etc.).

Normalization

If data were normalized/standardized, describe the approach(es): specify linear or non-linear and define image types used for transformation OR indicate that data were not normalized and explain rationale for lack of normalization.

Normalization template

Describe the template used for normalization/transformation, specifying subject space or group standardized space (e.g. original Talairach, MNI305, ICBM152) OR indicate that the data were not normalized.

Noise and artifact removal

Describe your procedure(s) for artifact and structured noise removal, specifying motion parameters, tissue signals and physiological signals (heart rate, respiration).

Volume censoring

Define your software and/or method and criteria for volume censoring, and state the extent of such censoring.

Statistical modeling & inference

Model type and settings

Specify type (mass univariate, multivariate, RSA, predictive, etc.) and describe essential details of the model at the first and second levels (e.g. fixed, random or mixed effects; drift or auto-correlation).

Effect(s) tested

Define precise effect in terms of the task or stimulus conditions instead of psychological concepts and indicate whether ANOVA or factorial designs were used.

Specify type of analysis: ☐ Whole brain ☐ ROI-based ☐ Both

Statistic type for inference

Specify voxel-wise or cluster-wise and report all relevant parameters for cluster-wise methods.

(See Eklund et al. 2016)

Correction

Describe the type of correction and how it is obtained for multiple comparisons (e.g. FWE, FDR, permutation or Monte Carlo).

Models & analysis

n/a	Involved in the study
☐	☐ Functional and/or effective connectivity
☐	☐ Graph analysis
☐	☐ Multivariate modeling or predictive analysis

Functional and/or effective connectivity

Report the measures of dependence used and the model details (e.g. Pearson correlation, partial correlation, mutual information).

Graph analysis

Report the dependent variable and connectivity measure, specifying weighted graph or binarized graph, subject- or group-level, and the global and/or node summaries used (e.g. clustering coefficient, efficiency, etc.).

Multivariate modeling and predictive analysis

Specify independent variables, features extraction and dimension reduction, model, training and evaluation metrics.